



**POLITECNICO**  
MILANO 1863

SCUOLA DI INGEGNERIA INDUSTRIALE  
E DELL'INFORMAZIONE

# Optimization and design procedure of a potassium Rankine cycle for Nuclear Electric Propulsion

TESI DI LAUREA MAGISTRALE IN  
NUCLEAR ENGINEERING - INGEGNERIA NUCLEARE

Author: **Luca Coita**

Student ID: 891734

Advisor: Prof. Stefano Lorenzi

Co-advisors: Prof. Pablo Rubiolo

Academic Year: 2021-22



# Abstract

A renewed interest in deep space exploration has grown over the last few years, and groundbreaking technologies are being investigated worldwide to get these challenging missions closer to feasibility. In the field of spacecraft propulsion, the Nuclear Electric technology (NEP) is seen as a future game changer. Thanks to the high power and specific impulse achievable, travel time and safety hazards associated with long-duration flights might be reduced. In a collaboration with the LPSC of Grenoble, this thesis work is part of the endeavor of implementing an optimization code capable of comparing different nuclear reactor concepts as well as power conversion systems (PCS) in order to provide the best engine configuration for any mission requirement. The focus is especially dedicated to the definition of a procedure aimed at determining the best Rankine cycle design from a system-specific mass (kg/kWe) point of view. By retrieving research activities from the early days of the U.S. space power program, the potentialities of such a thermodynamic cycle when combined with liquid metals such as potassium are presented. Moreover, the analysis points out the additional benefits of adopting a 1 MWth molten salt micro-reactor as a long-lasting and virtually maintenance-free power source. All thermal-physical calculations related to the cycle are performed using the Modelica language, which has been extended by including a specifically developed heat transfer model for potassium flow. The numerical results thus obtained are employed within a Python environment to create a metamodel version of the system, which is then processed to finalize the optimization. Outcomes show the PCS specific mass significantly decreasing down to 4 kg/Kwe with the increase of condenser temperature, which drives both the cycle and radiator efficiency. The latter confirms to be the most massive component for power outputs above 100 kWe, with cycle efficiency remaining a key parameter for trade-off analysis.

**Keywords:** Nuclear Electric Propulsion, Potassium Rankine cycle, Molten Salt Reactor, Liquid Metals, Modelica



# Sommario

L'esplorazione dello spazio profondo è stata protagonista negli ultimi anni di un rinnovato interesse che ha portato alla ricerca di tecnologie innovative in grado di rendere possibile questo genere di missioni così complesse. Nell'ambito della propulsione spaziale, quella nucleare di tipo elettrico è vista come un possibile punto di svolta: grazie alle alte potenze e al considerevole impulso specifico che è in grado di generare, i tempi di viaggio e i rischi associati a missioni di lunga durata possono essere apprezzabilmente ridotti. Attraverso una collaborazione con LPSC di Grenoble, questa tesi fa parte di un progetto per lo sviluppo di un codice di ottimizzazione capace di confrontare diversi modelli di reattore e di sistema di conversione dell'energia con l'obiettivo di definire, a seconda del carattere della missione, la configurazione propulsiva migliore. Nello specifico lo studio è dedicato all'individuazione di una procedura per determinare le condizioni ottimali di un ciclo Rankine dal punto di vista della massa specifica (kg/kWe) del sistema. Per cominciare vengono presentate le potenzialità di tale ciclo termodinamico combinato all'impiego di metalli liquidi come il potassio, ripercorrendo i risultati delle principali attività di ricerca svolte nei primi anni del programma spaziale statunitense. L'analisi prosegue mettendo in evidenza i benefici addizionali che l'adozione di un micro reattore a sali fusi da 1 MWth può garantire in quanto sorgente termica di lunga durata e praticamente auto-sufficiente. Per quel che riguarda la fisica del sistema, ogni calcolo è svolto grazie al linguaggio Modelica che è stato arricchito di un modello appositamente implementato per lo scambio termico del potassio. In seguito, i dati numerici così ottenuti vengono sfruttati in ambiente di programmazione Python per la creazione di un meta-modello, il quale viene a sua volta impiegato per finalizzare l'ottimizzazione. In conclusione i risultati mostrano che la massa specifica tende a diminuire fino a valori intorno a 4 kg/kWe all'aumentare della temperatura del condensatore che difatti stabilisce sia l'efficienza radiativa che quella dell'intero ciclo. Inoltre il sistema di raffreddamento costituisce il componente più pesante per tutte le configurazioni con potenza superiore a 100 kWe, per l'ottimizzazione delle quali l'efficienza totale resta un parametro essenziale.

**Parole chiave:** Propulsione elettrico nucleare, ciclo Rankine al potassio, Reattore a sali fusi, Metalli liquidi, Modelica



# Contents

<b>Abstract</b>	<b>i</b>
<b>Sommario</b>	<b>iii</b>
<b>Contents</b>	<b>v</b>
<b>Introduction</b>	<b>1</b>
<b>1 Nuclear Electric Propulsion</b>	<b>5</b>
1.1 SNAP-50 program . . . . .	8
1.2 Molten Salt Reactors . . . . .	10
1.2.1 Generation-IV reactors . . . . .	10
1.2.2 The MSR concept . . . . .	11
1.2.3 MSR for space propulsion . . . . .	12
1.2.4 The CNRS reactor design . . . . .	13
<b>2 Rankine cycle conversion system</b>	<b>21</b>
2.1 Introduction to the Rankine cycle . . . . .	21
2.2 Potassium working fluid . . . . .	22
2.3 System design . . . . .	23
2.3.1 System layout . . . . .	25
2.3.2 The heat transfer . . . . .	30
2.3.3 Boiler model validation . . . . .	38
2.4 Mass estimation . . . . .	41
<b>3 System optimization</b>	<b>47</b>
3.1 Optimization procedure . . . . .	47
3.1.1 Modelica Rankine cycle model . . . . .	47
3.1.2 Variable to optimize . . . . .	49
3.1.3 Metamodel creation . . . . .	54

3.1.4	Results . . . . .	57
<b>4</b>	<b>Conclusions and future developments</b>	<b>63</b>
	<b>Bibliography</b>	<b>67</b>
<b>A</b>	<b>Appendix A</b>	<b>71</b>
A.1	Saturation temperature . . . . .	71
A.2	Model explicit in pressure and enthalpy . . . . .	71
A.3	Model explicit in pressure and entropy . . . . .	75
<b>B</b>	<b>Appendix B</b>	<b>79</b>
<b>C</b>	<b>Appendix C</b>	<b>81</b>
C.1	Modelica components . . . . .	81
C.1.1	Source Mass Flow . . . . .	81
C.1.2	Flow-1DFV-2ph . . . . .	82
C.1.3	Metal-Tube-FV . . . . .	84
C.1.4	Counter-Current-FV . . . . .	85
C.1.5	Steam-Turbine-Unit . . . . .	86
C.1.6	Sink-Pressure . . . . .	87
C.1.7	Heat-Source-1DFV . . . . .	88
	<b>List of Figures</b>	<b>89</b>
	<b>List of Tables</b>	<b>91</b>
	<b>List of Symbols</b>	<b>93</b>
	<b>Acknowledgements</b>	<b>97</b>



# Introduction

## Space exploration

Being able to travel through space and explore new planets has always been one of the most fascinating experiences the human race has dreamed of. Several decades have passed since the 4<sup>th</sup> October 1957, the day on which the first artificial satellite was launched into space. It was a Russian metallic sphere, approximately 80 kg heavy that remained in orbit for about three months, and its name, Sputnik-1, means 'traveling together'. However, the *travel* for the space has quickly become a race, and in a few years we were able to step foot on the Moon and build our first space station, which allows us to see the Earth from a different perspective. And it is precisely a prospective change that is shaping the way we thought about space travel in the last few years. Research for new technologies aims to make any mission increasingly fast, long-ranged and cheap. Prompted by a renewed enthusiasm, worldwide space agencies have turned their attention to new destinations: Mars, Jupiter and beyond.

For a man to reach another planet is something that we have always wanted but never been able to do because of the technological challenges and human hazards involved. Wernher von Braun, NASA director in the seventies, was perfectly aware of those obstacles so he decided to bet on an extremely innovative and promising form of energy for a new spacecraft project: nuclear fission. Discovered just a few years before by the genius of Enrico Fermi, the idea of breaking atoms to produce energy for propulsion convinced physicists and engineers, who kicked off in 1961 the Nuclear Engine for Rocket Vehicle Application (NERVA) program. After only eleven years, political tension and budget reduction forced the program to come to an end. Nuclear energy had to wait for half a century before getting a second chance for a space propulsion application, once again thanks to NASA. In 2021, the American agency, in collaboration with the Department of Energy (DOE), funded three nuclear thermal space propulsion design concepts with 12-month-long contracts worth up to five million dollars apiece [33]. In the meantime, research activities are carried on to advance the readiness of another very popular technology, the Nuclear Electric Propulsion (NEP). With the latter, the propellant, instead of

being directly heated before expanding in the nozzle, is rather positively charged through electricity, generated by the reactor and then pushed out of a thruster.

According to NASA associate administrator Jim Reuter, all these designs could be "an important step towards tangible reactor hardware that could one day propel new missions and exciting discoveries". After years of improvement, nuclear technology is far more mature and might give that extra boost needed for a new giant *leap for mankind*.

## Objectives and outline of the thesis

One of the major obstacles that have so far prevented men from venturing into deep space is the transit time that such travel would require. To bring a manned mission closer to reality, the first obstacle to overcome is the reduction of flight duration, which in turn implies a mitigation of health hazards for the crew. Up to now, chemical propulsion has been the most widely adopted solution but its effectiveness decreases as mission distance grows. On the other hand, electricity from solar arrays suffers major drawbacks in terms of power and efficiency when the sun gets further away. Nuclear Electric Propulsion seems instead an attractive solution for deep space travel since the power provided to the thruster is not limited by fuel properties and an equal mass of propellant is used much more efficiently.

It is precisely a trade-off between mass and efficiency that underlies this whole thesis. Power plants on Earth are usually little concerned with mass or volume savings. Instead, on board a spacecraft, the lower the mass, the lower the thrust needed to move, and therefore every unit is made as light as possible. However, shrinking whatever system without affecting its performance requires enhancing its efficiency too. This explains why the specific mass, defined as the ratio between the system mass and the electric power produced, is such an important figure of merit for every kind of engine. In this work, the way in which the latter quantity varies with respect to different variables of a nuclear electric propulsion system is carefully investigated. The functional relations thus identified are then exploited to develop an optimization code, by means of which, the steps to define the best system design for every mission requirement are outlined.

This is a process that requires integrating lots of different aspects. On one side there is the reactor core with neutronic and thermal-hydraulic issues, on the other there is the propulsion unit, which deals with thrust and specific impulse and in between is a long list of systems necessary for energy conversion, heat rejection and power management. Since 2019, the Reactor Physics team at the *Laboratoire de Physique Subatomique et de Cosmologie* (LPSC) of Grenoble (FR) has committed to this task by working on the

design of a micro-reactor for NEP. Taking advantage of their long-time experience and thanks to the potential advantages of this concept, a molten salt reactor was chosen as the first candidate. Core mass minimization and both steady and transient conditions were analyzed over the past years, leading to the development of a tool able to perform a reactor-only optimization process.

To properly design a space propulsion system, however, the reactor is not the sole factor that must be taken into account, and several other components need to be studied in-depth. Nonetheless, it is crucial to know exactly how each of them behaves alone, before any coupling. This is the reason why, since last year, the work on power conversion units (PCUs), radiator design, electrical devices and also on different reactor types has been considerably growing at LPSC. The increasing interest in this project is also attested to by new partnerships with Politecnico di Milano, the *Centre national d'études spatiales* (CNES) and french startups as Hotblock. As part of this project, the study carried out within this thesis focuses on a potassium Rankine cycle power conversion unit. In particular, the definition of that configuration with the lowest specific mass is the ultimate goal of the implemented numerical optimization procedure.

The path followed to meet this objective is outlined as follows:

- **chapter 1** presents a brief overview of the nuclear electric propulsion features along with the description of one of the forerunner programs is provided. Later, the molten salt reactor concept developed at LPSC is presented as well as the way in which it is included in the framework of this study.
- **chapter 2** introduces the operating principle of the potassium Rankine cycle and the power conversion system layout focusing on the configuration of each component, its implementation within the modeling language Modelica and its mass estimation. Afterwards the development of a dedicated heat transfer model for potassium and its validation through result comparisons are discussed.
- **chapter 3** outlines the optimization procedure including an overview of the database and metamodel creation along with the employed Python algorithms. In the end, results showing the influence of different system variables on the specific and overall mass of the power conversion system are analyzed.



# 1 | Nuclear Electric Propulsion

The term deep space is usually referred to that part of space which is beyond the distance between the Earth and the Moon. Its exploration is not only one of the most commonly used sci-fi movies theme but also one of the most attractive field of aerospace research nowadays. Developing a better knowledge of deep space is considered the initial step to further understand the formation and evolution of the solar system as well as the relations among planets, stars and outer space. So far deep space mission have involved mainly robotic spacecraft or space probes with Voyager-1 being the farthest one humans have ever produced. However in 2013, NASA announced the name of eight astronauts who began a long training session for future mission beyond low Earth orbit [11]. This preparation, which involved also few ventures to the bottom of the Atlantic Ocean, allowed the crew to test exploration techniques meant for extreme environments such as those encountered during a planet landing.

To get an insight of a landing mission plan a subdivision into several phases is usually considered: the launch phase, the cruise phase, the approach phase and the entry, descent-and-landing (EDL) phase. For the sake of this work only a brief overview of the involved operations is given without delving into the depths of the subject. The first step is the launch of the spacecraft which comprises all the actions needed to carry the vehicle above Earth's atmosphere and to accelerate it to orbital velocity. A spacecraft is usually equipped with several-stages rocket as well as strap-on boosters. To date, combustion of chemical propellants seems the only viable way to produce the propulsive energy required for launching vehicles from Earth. Once escaped from terrestrial gravitation, the rocket's last stage burns out and separates, and just after that the cruise phase begins. In this phase, engineers on Earth monitor or calibrate spacecraft instrumentation and systems and at the same time they perform attitude and trajectory correction maneuvers to set the flight path.

So far almost every mission have relied on chemical monopropellant to operate the propulsion unit with bi-propellant being a possible alternative. When dealing with short range travels, these technologies proved to be the most efficient solution. However, as the flight

distance increases these options becomes more and more disadvantageous. Chemical fuel suitability mainly depends on two variables: the exhaust velocity and the propellant mass to the total vehicle mass. The attainable exhaust velocity for a propellant thruster is set by chemical bonds energy and thus, to raise it, the only way is to increase the amount of propellant. This requires to increase either the size of the spacecraft storage or the density of the propellant resulting in the need of mechanically stronger materials and higher building costs. Moreover, such a propulsion system can provide a powerful burst for a limited interval of time and once the fuel supply is exhausted there is little ability to speed up, slow down or change direction. In other words the spacecraft behaves as a bullet that can only go in the direction it's pointing when it accelerates. This implies that the mission is stuck into specific launch windows and orbital departure timeframes as its path can only be slightly corrected along the way [28]. For all these reasons, at the moment, only robotic explorers or automated spacecrafts traveled to planets like Mars or Jupiter, since there is no need of a comeback. In fact, waiting for optimal planetary alignment for the return trip would require astronauts stretch their round-trip to more than three years.

Electric propulsion instead seems to deliver some attractive solutions to those problems. It converts energy into electricity and uses it to ionize, or positively charge, inert gas propellants like xenon and krypton, and then to accelerate them through electric or magnetic fields. Since the power source of an electric thruster is not fixed by the fuel properties, the ions can be ejected at higher exhaust velocities. Also, the propellant mass can be reduced if the power source efficiency is higher than the one of fuel combustion. Both these peculiarities make this technology well suited for low-thrust and long-duration space applications. As described by Jimi Russell from NASA Glenn Research Center [28], an electric propulsion vehicle, once launched in space, is "out for a cross country drive", it can accelerate or slow down for years, limited only by the gas in the tank. This can reduce the time travel and minimize the surface stay, making this kind of technology very attractive.

Thanks to their flexibility, several Electric Propulsion Systems (EPS) have been developed which basically differ in the used thruster: Gridded Ion Engine, Pulsed Plasma Thruster, Hall Effect Thruster and so on. The choice among them is strictly related to the specific mission requirements and also for the same application, trade off analysis must be performed to identify the most attractive technology. The performance of a thruster must be defined according to multiple aspects that can be summarized by a set of four parameters: specific impulse ( $I_{sp}$ ), thrust efficiency ( $\eta$ ), specific mass ( $\alpha$ ) and lifetime [21]. Specific impulse is defined as the thrust per unit weight of propellant flow, measured at sea level:

$$I_{sp} = \frac{T}{m \cdot g_o} = \frac{u_e}{g_o} \quad (1.1)$$

where  $m$  is the propellant mass flow rate,  $T$  is the engine thrust ( $m \cdot u_e$ ), and  $g_o$  is the acceleration due to gravity at sea level. Thrust efficiency ( $\eta$ ) is the ratio of the kinetic power useful for thrust to the electrical power input to the thruster:

$$\eta = \frac{\frac{1}{2}u_e \cdot T}{J \cdot V} = \frac{\frac{1}{2}I_{sp} \cdot g_o \cdot T}{J \cdot V} \quad (1.2)$$

where the electrical power is the product of the total current ( $J$ ) and the voltage ( $V$ ) input to the thruster. Specific mass ( $\alpha$ ) is the ratio of the power and propulsion system mass to the electrical power generated and Lifetime is the length of time the thruster can operate before failure. Without getting into detail, it is evident that being able to generate the highest thrust using the lowest system mass possible is paramount to obtain an effective thruster [29].

Among the different power sources the most adopted one is the radiation of the Sun. In fact, Solar Electric Propulsion (SEP) plays a key role in a number of applications, as station keeping on geostationary satellites, but it rarely operates at more than tens of kilowatt. Unfortunately the thrust that can be extracted from such an amount of electrical power can be quite limiting. Moreover, the efficiency of solar panels inherently decreases with the square of the distance from the Sun due to the weaker solar radiation intensity affecting the liability of this energy source for deep space mission. The alternative option which is also the subject of this work is the nuclear energy. The use of a fission reactor can be considered a possible game changer for not-so-distant future space exploration. For instance a combination of chemical and nuclear electric propulsion might considerably reduce the expedition transit time which is a major issue of any interplanetary space travel [23]. For manned mission, this would mean to mitigate the health hazard for the crew, minimizing the duration of exposure to space radiation and microgravity conditions [29]. At the same time a nuclear reactor on board of a spacecraft could be an uncommon trip mate to share the flight with. Control issues, mechanical stresses, required maintenance and so on are factors that must be accounted and foreseen. However before focusing on the design, we take a step back in time to look at one of the leading nuclear electric propulsion project.

## 1.1. SNAP-50 program

Among the reactors having given a great boost to the development of a new generation of space propulsion systems the SNAP-50 is probably one of the most significant. It was the last, and most powerful, of the SNAP series of reactors and during its life it has been part of quite different research programs. It started as the Aircraft Nuclear Propulsion program (ANP) power source for the US Air Force and it ended being part of a power plant for future modular space stations planned by NASA in the 70's. Even if it was quite twisty, this road trip made its fortune since the SNAP-50 innovative layout permanently altered the way that astronuclear reactor were designed for almost the following twenty years [1].

Back in the early days of the space era, the atomic energy appealed lots of propulsion programs. Yet in 1955 the System for Nuclear Auxiliary Propulsion, also known as SNAP, program was launched with the aim of covering a wide range of transport and exploration fields. To make a clear distinction, SNAP was divided into an odd and even numbering scheme: the odd model numbers being radioisotope thermoelectric generators and the even one including fission reactor electrical power systems. Among the latter one can mention the SNAP-2, developed to become a competitor to the Sputnik-1 satellite or the SNAP-4, designed for submarine propulsion. Despite the range of applications, there is a number of similarities in almost every SNAP designs. All the reactors adopted the same type of fissile fuel, the Uranium-Zirconium hydride (U-ZrH). This fuel was very popular at the time but still today it offers several attractive features, as the self-moderation, that make it widely used for TRIGA reactors. Most of the SNAP design were initially cooled also with the same liquid metal, NaK, and connected to the same power conversion system: a boiling mercury Rankine cycle. This shared basis guaranteed several advantages since improvements for one reactor could in principle be extended to the others. Similarly, issues appeared in a reactor and not in the others helped the engineers exchange results and ideas on how to solve problems and improve the design. Nonetheless this strategy represented at the same time kind of an obstacle to the introduction of completely new technologies. Fortunately, another program was going on about in the same years with a very different purpose but similar enough design constraints: the Aircraft Nuclear Propulsion program[1]. The ANP program was originally rounded out at the Oak Ridge National Laboratory where it became famous for Project PLUTO series of ramjets: the TORY series. These engines were powered by nuclear energy and used the atmosphere itself as working fluid. This last feature was probably the most challenging one, since in case of failure of the cladding, fission product would have been released similarly to a



nuclear fallout event. To overcome these issues researchers working for the ANP proposed as alternative approach an indirect cycle, in which the reactor was meant to heat a working fluid in a closed loop, which in turn heated another fluid before transferring heat to the air. This configuration is way safer but also far more massive and less efficient, requiring for higher power and temperature to reach the necessary thrust-to-weight ratio for the aircraft. However these requirements were the channel that made it possible for SNAP and ANP projects to encounter. Both of them were seeking for a nuclear reactor to be compact and lightweight but also with a very high power density and the capability to operate nearly maintenance-free in most of the high-power conditions. The ANP selected design was firstly developed at the Connecticut Advanced Nuclear Engine Laboratory (CANEL) in Middletown, and the prime contractor was Pratt and Whitney. Lots of challenges related to the indirect-cycle set back the project, eventually leading to its cancellation in 1961. Overnight Pratt and Whitney found themselves without a customer for their reactor despite the extensive testing already done and the novel alloys fabrication. However, it didn't take them long to find a new partner: both NASA and US Air Force were interested in a high powered reactor for their in-space projects. The next year they joined forces and finally gave birth to the SNAP-50 [3].

Since its foundation the SNAP program was intended to develop a nuclear electric power system suitable for a range of applications. At NASA the main interest was in finding a technology able to provide an adequate amount of energy for the space station they were foreseeing to build. Once space became a realistic place to send not only scientific payloads but personnel, semi-permanent station provided with centrifugal gravity and housed by dozens of individuals seemed close to feasibility. To meet the energy demand of such a massive spacecraft, engineers had to set aside the thermoelectric conversion system (adopted in the previous SNAP-2 and SNAP-8 design) in favor of a more efficient Rankine cycle.

Among all the design innovations, the SNAP-50 reactor owes its importance mainly to: its fuel and its coolant. Several experiments were performed to test different fuel types: in fact uranium carbide (UC) can stand the highest operating temperature but after all it was discarded in favor of uranium nitride (UN) which has the highest fissile density with respect to any solid fuel [7]. No less important was the coolant choice and unlike its predecessors, this design borrowed from the PWAR test reactor series, a at-the-time unique coolant: the lithium. Compared to the NaK, liquid lithium has a three time higher specific heat capacity which means higher amount of energy contained as heat per unit mass at a given temperature. A less amount of fluid mass is then needed to transfer heat from the reactor to the power conversion system. Moreover it is far less massive than NaK

and this makes it a highly coveted option for astronuclear reactor design. In the Rankine cycle the lithium, once heated, would feed into a potassium boiler before being returned to the reactor core. Out of the boiler the potassium vapor would enter a Rankine turbine producing electricity. To cool down the working fluid a set of radiator was envisaged to return it, condensed in liquid form, to the boiler inlet. This design was meant to operate in both single or dual loop configuration with an identical second loop used to manage high-power operations and increase redundancy [2]. This flexibility perfectly embraced NASA ambitious plan which required both a 35 kW system for smaller space stations or lunar bases and a larger 300 kW type for modular space station project (which eventually evolved into the actual ISS). Thus boiler, pumps and radiators were tested past the 10,000 hours power plant design lifetime and all the major arisen complications were addressed proving the system to be ready for the in-flight test configuration.

Unfortunately this test never started: while these higher-powered reactor designs were coming to maturity, funding for space programs virtually disappeared. New national priorities, the shift from crewed to uncrewed missions, the transition from Atomic Energy Commission to Department of Energy and the rise of Space Shuttle placed a whole different set of constraints on the reactor, that would have required to rewrite the design from its very basis. All these changes spelled the death of the SNAP-50 program in 1973 and we had to wait for ten years to see again a nuclear reactor system involved in a space application program, the SP-100. But here this introduction comes to an end: after a quick view of the design that inspired this work Rankine cycle, now the focus shifts on the reactor concept.

## 1.2. Molten Salt Reactors

### 1.2.1. Generation-IV reactors

Established in 2001, the Generation IV International Forum was created as a co-operative international endeavour with the aim to test feasibility and performance of a new generation of nuclear systems in order to make them available for industrial deployment by 2030 [12]. As a collective it brings together 13 countries (as United States, Russia, China and UK) and Euratom, representing the 27 European Union members, to coordinate the development path. Its first assignment was indeed to identify the most noteworthy reactor technologies deserving new research and fundings. Six different reactor prototypes were included into the Generation IV list and almost all of them are actually concepts studied since the early 1960's. However, one of them has a history that dates even further back in time: the Molten Salt Reactor (MSR).

The first research program devoted to MSR's started as part of the already mentioned Aircraft Nuclear Propulsion program, a joint project between Air Force and Atomic Energy Commission. At the time U.S. military was interested in an ultra-lightweight reactor to be put on an airplane that could stay airborne for several weeks. A land-based 2.5 MWt reactor was built and tested in 1954 and a 60 MWt prototype design was on its way when the program was canceled in favor of ICBM (Intercontinental Ballistic Missile) technology. Despite of that, the work on MSR's proceeded at ORNL where the focus was shifted from military to civilian applications. Several experiments showed that MSR's were suitable to breed U-233 from Th-232 in an efficient way with a thermal neutron spectrum [14]. A 7.4 MWt reactor was then built in 1964 and it operated for 5 years permitting the engineers to collect tons of data regarding fission products behaviour, handling of fuel and more. Nonetheless the project was halted in the late 1970's and research into MSR's slowed down but never stopped.

### 1.2.2. The MSR concept

The inclusion of MSR's among the Generation IV reactor systems, sparked a renewed interest in this concept. It's a technology which has so many advantages that make it a remarkable option for a variety of application, with the space propulsion as one of the most fascinating [9]. Molten salt reactors are quite different from any conventional reactors and their uniqueness lies in the special fuel they use [8]. The fissile material indeed is not in a solid form, instead it's dissolved in a molten salt which acts also as a coolant and constantly circulates through the core and other systems. The salt could be a fluoride or chloride one or even a mixture with lithium or beryllium. In the core, fission reactions generate heat that is eventually transferred to a power conversion system. In order to keep circulating, the fuel must remain in liquid form, which means above its melting point: this temperature limit is usually in the range between 700 K and 1,100 K for most of the salt adopted. For a traditional reactor, it is technologically challenging to reach such high temperatures with high neutron fluence since solid fuels are easier to swell, crack and interact with the cladding. Instead the cavity of a MSR vessel is almost entirely free of internal structure that could be damaged. This also implies a benefit for the reactor burn-up which is usually limited by the fuel-clad lifetime. In a molten salt reactor such a limit doesn't exist thanks to the lack of any fuel cladding. Reducing internal support structure means a reduction in neutron leakage. Less parasitic absorption is another advantage that makes this concept neutronicly appealing, allowing for higher burn-up and smaller critical sizes.

In addition molten salt reactors are characterized by a large negative temperature reac-

tivity feedback. The liquid fuel, when heated, expands rapidly and a portion of molten salt is pushed outside the core, lowering the amount of fissile material in the core itself. In case of severe events, whether the fuel is heated faster than thermal expansion reaction, the boiling of the liquid fuel will bring the reactor in a subcritical state avoiding any damage at the structure.

Finally, molten salt reactors are designed in a way that the fuel can be handled quite easily. Implementation of online refueling is simpler with respect to solid fuel reactors, since it doesn't require dismantling and core reconfiguration. Moreover noble gases, notable neutron poisons like Xe-135 and Kr-83, can be removed continuously from the reactor by sparging the fuel with helium.

The amount of precursors nuclei decaying outside the core is usually a concern for MSRs. Precursors behaviour directly affects the delayed neutron fraction which has to be as high as possible to maintain the reactor controllable. To maximize the amount of delayed neutrons it is necessary to maximize the time spent by the fuel in the core and minimize the time outside of it. For a given core volume this requirement becomes more and more difficult with increasing power since the fuel salt must flow quicker to transport heat to the heat exchanger. Therefore it is of pivotal importance to have an efficient heat exchanger that can rapidly transfer heat from the fuel to the power conversion system.

### 1.2.3. MSR for space propulsion

So far the features making the MSR an appealing concept have been described but the reasons for considering it an interesting choice for space propulsion systems haven't yet been claimed. To do so, it's useful to remind some considerations about space flight and simple laws of physics.

First of all it's important to understand why is so crucial for a spacecraft to be as light as possible and therefore the concept of thrust must be clarified. The thrust is the force per unit area that moves any aircraft. An aeroplane uses turbines to push air backwards and to gain the necessary thrust in the forward direction. Similarly a spacecraft forces gases or ions out of the exhaust to get driven through the space. A spacecraft engine behaves as similar as a balloon filled with air. If the balloon neck is released, the pressure gradient pushes out the air with some force, and an equal and opposite force acts on the balloon which flies forward. The effect for which every action causes an equal and opposite reaction is nothing but Newton's Third Law of motion. Almost all the propulsion system are based on this law. The distance travelled by the balloon depends on the thrust  $F$  which is directly proportional to the ejected amount of propellant per unit time  $\dot{m}$  and

to its exit velocity  $v_e$ .

$$F \propto \dot{m} \cdot v_e \quad (1.3)$$

However the same force, being inversely proportional to the mass, will grant lighter bodies an higher acceleration. These considerations are primarily of concern when it comes to put objects beyond low earth orbit. The high cost of these missions forces to find power systems with low specific masses and nuclear fission systems are optimal, thanks to their extremely energy-dense fuel. In addition, molten salt reactors are somewhat sparing of internal structures and this places them among the design with the highest core average power density:

$$Q''' = \frac{Q_R}{V_{core}} \quad (1.4)$$

where  $Q_R$  is the power produced by the reactor (kW) and  $V_{core}$  is the core volume (m<sup>3</sup>). The core average power density represents an important figure of merit when it comes to design a reactor since it's not related just to the fuel choice but also to core layout and materials. Even if this parameter seems not directly in relation with the mass of the system, it must be considered that one of the most massive component in compact reactor design is the core shielding. By limiting the core volume one can also reduce a lot the shield structure and so the system mass. For this reason, a MSR is usually able to provide a higher output power with respect to a solid fuel reactor with the same mass. Otherwise it can be far lighter than a solid fuel reactor with the same output power. However MSRs relatively-high power density is not enough to make them a good reactor concept for Nuclear Electric Propulsion. Their unique design indeed offers some other intrinsic advantages for in space applications. To high power density, MSRs combine high temperatures with low fuel pressure and low temperature gradients which assist in enhancing operating performance and to a lesser extent also in reducing mechanical requirements [9]. Moreover, at least for a compact design, the reactivity feedback coupled with simple control systems improve the overall reactor reliability making it an almost self-regulating and maintenance-free system.

#### 1.2.4. The CNRS reactor design

All these promising features convinced the French National Center for Scientific Research (CNRS) to carry out design studies for a NEP engine based on a MSR. Actually, the CNRS isn't completely new to MSR research; since 2004, their LPSC reactor physics department

in Grenoble is actively involved in the development of a particular MSR design called Molten Salt Fast Reactor (MSFR) [27]. As opposed to thermal molten salt reactors, the MSFR does not employ any kind of moderator which results in a fast-spectrum breeder reactor. Even if this 3,000 MW<sub>th</sub> design is very distant from any possible NEP engine concept, several years of studies and experiments have made the French research center one of the more experienced in this field. For this reason, the reactor branch decided few years ago to convey its expertise to a new project aimed at developing a Nuclear Electric Propulsion engine based on a Molten Salt Reactor [26]. Different configurations are currently being studied but within this work a fast neutron spectrum concept is investigated.

Molten salt reactors allow to exploit core geometry which are usually less doable with solid fuel. The CNRS decided to resume a spherical core geometry similar to the one proposed in the ANP project. The layout showed in fig. 1.1 is particularly efficient for lots of aspects: it permits to minimize the neutron leaks as well as the shielding requirements and it also improves the core cavity flow distribution. The hot molten salt is supposed to be extracted from the top of the core thanks to six pipes located in an external ring. Here the fuel passes through Heat Exchangers before a system of pumps pushes it back into the core cavity through six pipes that generate a jet oriented from the top towards the walls. A thermal insulation layer made of carbon foam is placed between the cavity cladding and the reflector.

For this concept, the employment of different molten salts was compared. The type selection has indeed a significant impact on the reactor performance given that the salt acts not only as fuel but also as core coolant. Among the salt properties that play a key role, the melting temperature is the major responsible for the minimum core operating temperature. A salt with a low melting point provides a large range of operating temperatures and a simpler startup procedure. On the other hand the core critical mass is influenced by the salt density and heavy metal solubility, therefore salts which grants higher fissile solubility are more suited to minimize the core critical mass. Moreover, salt viscosity determines the pressure losses in the fuel circuit hence the required pumping power, however this shouldn't be a concern for compact reactors. With regard to control, a large thermal expansion coefficient is usually preferred since it implies a larger reactivity feedback coefficient. All these considerations led to the conclusion that an eutectic molten salt based on LiF-UF<sub>4</sub> (molar composition 73.4% LiF and 26.6% UF<sub>4</sub>) would be a good fuel carrier for a fast spectrum reactor. Uranium 235 was chosen as fissile material rather than plutonium 239 because of the relatively low chemical and radiotoxicity of the former. Even if two distinct levels of fuel enrichment (20% and 92%) were originally studied, re-

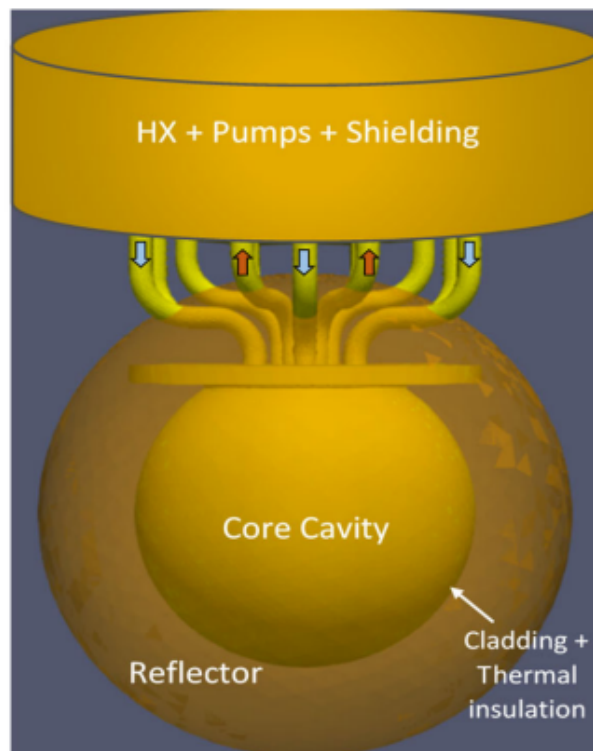


Figure 1.1: Layout rendering of the space MSR core with a fast spectrum [26].

searchers at CNRS agreed with most of the nuclear experts upon the fact that only Low Enriched Uranium (LEU) fueled space reactors constitute a viable option for developing nuclear power in space, due to proliferation concerns. Once the fuel and its enrichment level have been chosen the minimum core critical mass is estimated. The lightest possible reactor core with a spherical geometry was obtained which is consistent with the aim of this work. At last, to achieve the highest power density, compatible with the materials, thermal power is set to 1 MW. The main parameters of this LEU molten salt reactor are reported in table 1.1 and have been used to estimate the overall system mass as described in the following chapters.

As concerns the material used for the core cladding and the other reactor components, the refractory alloy Molybdenum TZM has been selected for this concept. TZM (Titanium-Zirconium-Molybdenum) is an alloy composed of 0.50% Titanium, 0.08% Zirconium and 0.02% Carbon with the balance Molybdenum. While molten salt could operate in theory at temperatures that overcome 1,250 K, corrosion of structural materials in contact with the salt limits the maximum operating temperature. Because of this, TZM has been tested for long at ORNL showing negligible corrosion by fluoride salt up to 1,350 K. Nonetheless, to retain some margin, the maximum molten salt temperature is set to 1,200 K. However this temperature would be unbearable by the core if some precautions weren't

Dimensions	
Core cavity radius (cm)	35
Cladding thickness (mm)	8
Reflector thickness (cm)	23
Core component masses	
Molten fuel salt (kg)	1,003
Cladding (kg)	344
Reflector (kg)	1150
Core operating conditions	
Thermal power (MW)	1
Molten salt flow rate (L/s)	3.6
Core temperature rise (K)	52

Table 1.1: Main MSR parameters [26].

taken. In fact, core reflector, whose material choice is crucial to minimize the critical core mass, is the component exposed to the higher neutron fluence. In fast MSRs typical values calculated in the radial reflector can be as high as  $10^{21}$  n/cm<sup>2</sup> which is enough to cause neutron damage as irradiation swelling over 3-5%. To avoid it one can either reduce the neutron fluence itself by limiting the core power density, hence worsening the reactor performance, or by keeping the reflector temperature below some safety threshold that depends on the material adopted. For the CNRS design two different materials were found to guarantee the best core mass optimization, Beryllium (Be) and Beryllium oxide (BeO). The former was preferred thanks to its better neutronic performance despite a lower melting point (1,560 K versus 2,820 K). Anyway the latter is not a big issue since to prevent Beryllium from serious swelling, it must be kept below 800 K. To do that without penalizing the fuel working conditions and by avoiding strong temperature gradients in the cladding, which could cause important mechanical stresses, a thermal insulation is placed between the cavity cladding and the reflector. Without this carbon foam layer coating the cavity, the reactor wouldn't be able to reach its life duration target.

The CNRS reactor is expected to operate for 10 years and during this period of time material irradiation is not the only issue that must be predicted. Along its lifetime reactor overall reactivity is going to decrease due to fuel depletion, plutonium generation and accumulation of fission products such as xenon, samarium and others. Using the MCNP code, core burnup calculations were performed finding out that reactivity evolution is



nearly linear and that total core reactivity swing is about -2,000 pcm, with a Monte Carlo uncertainty error of about 11 pcm (fig. 1.2). The reactivity swing is defined as the reactivity difference between beginning-of-life and end-of-life of the reactor, and such a relatively small value is mainly due to the low burnup achieved in the fuel. However, if no control strategy were applied, this amount of reactivity would be sufficient to decrease the molten salt temperature of more than 500 K over the 10 years reactor operation.

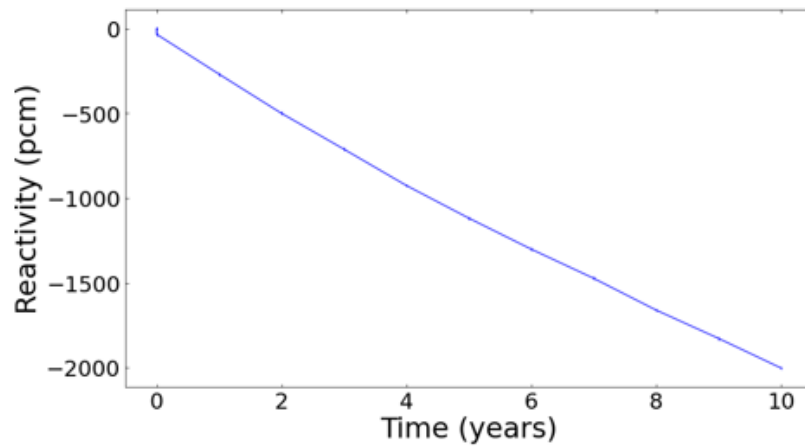


Figure 1.2: Reactivity swing of the LEU fast MSR due to the fuel burnup. Reactor thermal power set to 1 MW over the 10 years of operating time [26].

To counter balance this reactivity decrease, traditional reactors usually rely on control rods. However, molten salt fuel offers the opportunity to still simplify the reactor design. In fact, it's under investigation the possibility to get rid of control rods in favor of other passive control system. A first idea was to increase the volume of molten fuel salt outside the core which would help decreasing the effective fuel power density and burnup. Nonetheless, that option was discarded since molten salt fuel volume is already relatively large (180 litres in the core and 50 litres outside the core). Another option involves the use of a burnable poison as Boron, Gadolinium or Europium which has a capability of capturing neutrons that decreases in efficiency along with reactor lifetime. Several studies proved that Boron, added as a coating over the cavity cladding or in the thermal insulation, shows an excellent reactivity control performance. For sake of simplicity, simulations were performed in which the poison was homogeneously mixed with the TZM cladding material and concentration of 0.07% of Boron atom showed to limit the reactivity swing to about 170 pcm. Moreover, in these calculations fission gases were simply considered as gases mixed in an homogeneous way with the molten salt and nor their behaviour nor any removal strategy was considered. This does not allow to predict correctly the pressure evolution in the fuel circuit but at least it's a conservative choice from the reactivity point

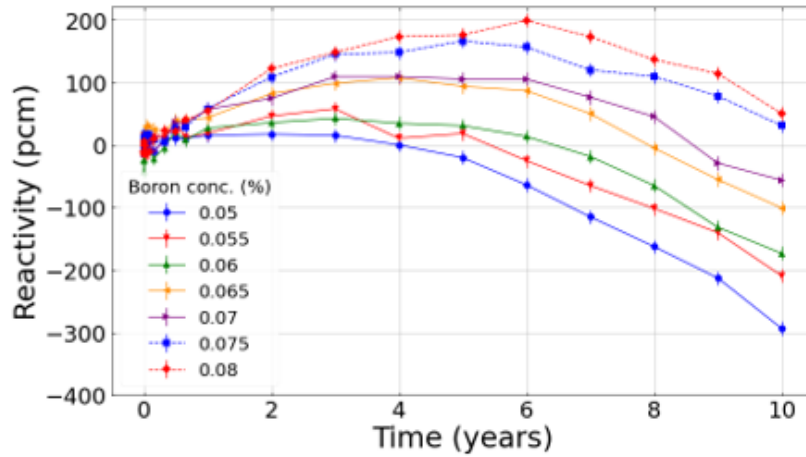


Figure 1.3: Reactivity swing over time with different boron concentrations [26].

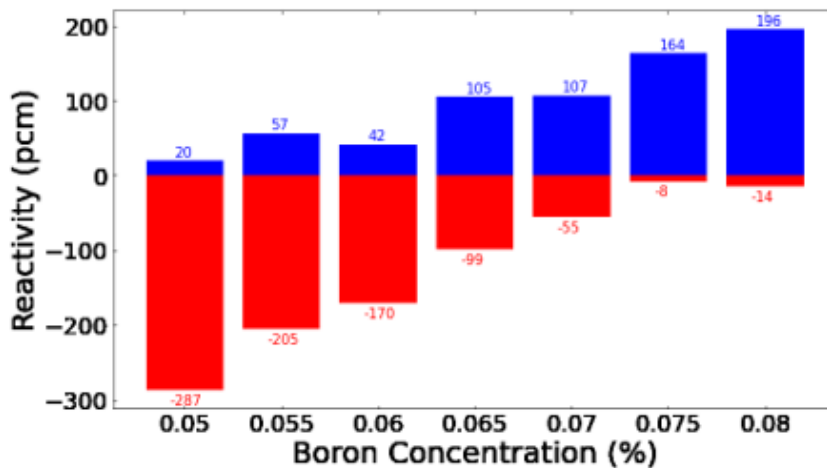


Figure 1.4: Maximum and minimum reactivity swing as function of boron concentration [26].

of view, since fission gases removal would slightly decrease the reactivity swing.

To better understand how the reactivity is going to influence the fuel temperature over the years of operation, fuel temperature feedback coefficients, Doppler and density effects, were evaluated at CNRS for the LEU MSFR. These coefficients, whose estimation is paramount to be able to maintain the reactor critical, were calculated with the Monte Carlo code *SERPENT 2* without considering any core cavity change in size. Thermal expansion coefficient of the TZM alloy is indeed significantly lower than the one of the molten fuel salt, whose change of density was instead taken into account. Results show fuel temperature coefficient ranging from -3.7 pcm/K at Beginning of Life (BoL) to -3.9 pcm/K at End of Life (EoL), which means a maximum fuel temperature variation below

50 K. This outcome that is encouraging from the reactivity control point of view could instead have some non negligible impact on the power conversion system as well as the heat rejection one. After this

To conclude the reactor concept overview, it's worth mentioning the strategy under study for the system start-up. The reactor is expected to be kept in sub-criticality conditions until it's in a safe orbit. To accomplish that, the molten fuel salt should be stored, during the launching, into six separated tanks of about 40 litres each at a temperature above the critical one. Once the reactor is ready to be started, the tanks can be drained into the core cavity where the reactor would reach the criticality condition only when the molten fuel salt has been sufficiently cooled down in the heat exchangers.



# 2 | Rankine cycle conversion system

## 2.1. Introduction to the Rankine cycle

So far, the reactor core has been described, but the remaining parts of the power system that are strictly coupled to the MSR have only been mentioned. As already highlighted, electric propulsion requires energy to ionize or positively charge inert gas propellants, therefore, within the engine, a crucial element is represented by the Power Conversion System (PCS). This system is aimed at converting thermal power, produced by a heat source, into electrical power that can be immediately used or stored. The conversion unit is not an unconventional system since every power plant on Earth, whether nuclear or not, is equipped with one or more PCSs. Most commercial systems are based on the Rankine or Brayton cycle, which have both been considered since NEP was developed in the 1960s [25]. However, for reasons that will be clearer at the end of this section, the Rankine cycle was found to have the highest potential for application to high-power nuclear systems, both for spacecraft and surface power stations [16]. The Rankine cycle relies on the extraction of energy from a vapor-phase working fluid via a turbine coupled with an alternator. The turbine exhaust vapor is then condensed into liquid and pumped back through the heat exchanger, where it gets vaporized to repeat the loop. It's a technology applicable over a wide range of power levels, with cycle efficiencies that can be as high as 30%. The most widely adopted configuration is the indirect or two-loop one, in which the heat source is on the primary side and the other components on the secondary one. The direct cycle or single loop system, in which the vapor phase is generated directly at the primary heat source, is just as common. Even if this design is mechanically simpler and less massive, we cannot get rid of the secondary circuit since we are dealing with a molten salt reactor in which the coolant also acts as fuel. At this point, it's important to clarify that the power conversion system that is investigated in this work isn't intended for a molten salt reactor only. Although this preliminary optimization procedure has been applied to a Rankine cycle coupled to a molten salt reactor, the same system could be

employed for other types of reactors by simply adjusting the primary side. In the next few years, further analysis will be devoted to lead-cooled fast reactors as well as heat pipe-cooled reactors, but in those cases, the same consideration about the non-feasibility of a single loop configuration can be made.

## 2.2. Potassium working fluid

The major difference between terrestrial power conversion systems and space ones is related to the employed working fluid. Whereas water is the most widely adopted fluid on Earth, alkali metals are the main choice for space applications thanks to the technical advantages they offer. Liquid metals claim large thermal conductivity, small kinematic viscosity, small vapor pressure and a wide high-temperature range over which they remain in the liquid phase. Therefore, they are considered efficient heat transfer media in processes with limited heat exchange surfaces and exceptionally high thermal loads [30]. Potassium, in particular, can boast favorable thermodynamic properties that contribute to reaching a high cycle efficiency. Moreover, it can work within a large range of temperatures without significantly increasing the operative pressure and this implies more compact components, which means a higher system-specific mass [22]. Compared to other alkali metals, potassium proved to also have a higher boiling stability as well as the lowest tendency for erosion on turbine blades. All these advantageous features make this metal the best option for an advanced space Rankine cycle such as the one investigated in this study.

To perform all the thermodynamic calculations, the object-oriented modeling language Modelica-DYMOLA is used. Modelica has several libraries, designed to model and simulate complex systems that span multiple engineering disciplines. As will be further described in the next section, this tool allowed for the creation of a complete Rankine cycle model that assisted in creating a database of hundreds of different cycle configurations. Although most of the components employed in a conversion system, such as heat exchangers, turbines or pumps are already implemented in Modelica libraries, a model for a potassium medium is not present. Fortunately, the Dymola environment is completely open and its users can easily introduce new components from scratch or by using existing ones as templates. Therefore, a specific model based on the two-phase-media one was developed. This required looking for potassium thermodynamic properties encompassing the widest possible range of temperatures that comprise liquid, vapor and two-phase states. However, the amount of data on potassium boiling is very small and limited to few experimental activities carried out in the 1960's. Whenever it was not possible to

retrieve already developed correlations, approximated equations were constructed by interpolation of available data [20] [10] [5]. The latter equations will also be recognized among the others by the presence of the coefficient of determination  $R^2$  which provides a measure of how well observed outcomes are replicated by the equation itself.

In appendix A.3, a summary of all the equations collected and developed for the estimation of potassium properties is reported. Most of them define a relationship between a thermodynamic property and fluid temperature. However, the employed Modelica components require in some cases a fluid model that is explicit in pressure and specific enthalpy and in others a fluid model that is explicit in specific entropy and pressure. For this reason, the potassium code is divided into two branches, each one implemented in a way that, from the corresponding couple of input variables, the temperature state could be firstly evaluated and only successively employed to define the objective property. It is worth underlining that, even if a distinction between the two model is made, the one explicit in entropy is implemented such as that an evaluation of the enthalpy state is done right away through adequate correlations in order to go back to the other model set of equations.

Moreover, the potassium state is divided into three main regions: two single-phase regions, liquid and vapour, and a two-phase region. Each of these regions has a different set of equations. Within the model, region identification is simply based on an enthalpy or entropy evaluation. For components that require a fluid model explicit in pressure and specific enthalpy, the procedure is the following: if the specific enthalpy is lower than the one of the saturated liquid at the same pressure, then the fluid is considered to be in the liquid region. Whether its specific enthalpy were higher than the saturated vapour one at the same pressure, then it would be in the vapor region. In any other situation, the fluid is considered to be in a two-phase region. The same reasoning applies for a component requiring a potassium model explicit in pressure and specific entropy. In this case, the threshold values are represented by the specific entropy of saturated liquid and the one of saturated vapor evaluated at the fluid pressure.

Due to the shortcoming of data on boiling potassium, the verification of such a code was done by replicating experimental setups, coming from research activities, on Modelica and verifying the outcomes agreement. Optimal results were achieved for temperature and pressure ranges reported in table 2.1.

### 2.3. System design

The numerous advantages that a Rankine cycle in which liquid metals are adopted as working fluids can boast have been described. However, the way in which the high oper-

Variable	Range of values
Potassium temperature (K)	750 - 1500 K
Potassium pressure (bar)	0.1 - 20

Table 2.1: Verified ranges of applicability of the reported equations.

ative temperatures characterizing such a technology can impact the system mass is still to be discussed. Among the different components, the one with the greatest benefit is the heat rejection system. Radiators performance is indeed proportional to the difference between their temperature and the ambient one. Since space temperature cannot be controlled, an increase in radiator one leads to a better rejection capability per unit area of radiator. Nonetheless, a higher sink temperature means a worse cycle efficiency, so a trade-off study is required to maximize the performance and minimize the mass of the whole heat rejection system (HRS).

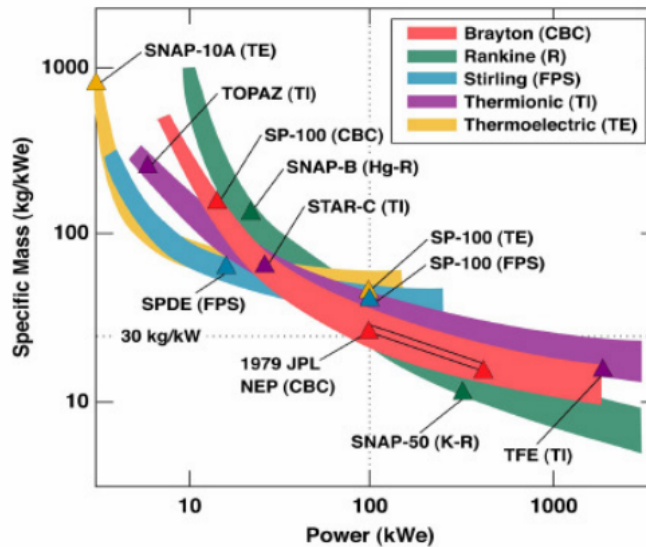


Figure 2.1: System specific mass as function of electric power produced [31].

A lesser need for radiator surface is just one of the arguments that makes the Rankine cycle more convenient with respect to single-phase conversion systems. The working fluid phase change not only allows more thermal energy per unit mass to be transported through the circuit but also implies a heat rejection process at constant saturation temperature. This latter condition is particularly favorable once liquid metals are employed thanks to their capability to operate at high temperatures with low system pressure. As it can be seen by a comparison of different power conversion designs, including the one adopted by the above discussed SNAP-50 (fig. 2.1), the positive effects are mainly evident for power levels



greater than 100 kWe, and this makes potassium Rankine cycles the leading candidates for high-power space conversion systems [31].

Once again, it's clear that mass reduction is the driver of almost every technological choice in this advanced design. The importance of this parameter over any other has already been underlined, and for this reason, its assessment represents the starting point for system optimization.

### 2.3.1. System layout

At the beginning, the simplest indirect Rankine cycle configuration has been considered (fig. 2.2): a primary loop filled with  $\text{LiF-UF}_4$  is connected to the secondary one through a heat exchanger in which liquid potassium is heated up until it reaches 100% vapor quality. A steam turbine is placed downstream, and eventually a condenser coupled to a heat rejection system returns potassium to the liquid phase. As a preliminary work, any employed component is the very standard one and no attempt was initially made to improve their efficiency and performance. All the efforts were devoted to finding a configuration that was at least compatible with the thermal and mechanical constraints imposed by the cycle. To model it, the already-introduced object-oriented modeling language Modelica-DYMOLA has been used. The code libraries, and in particular the *ThermoPower* one, developed at Politecnico di Milano [4], already have all the required component models except for the potassium medium that has been discussed in the previous section.

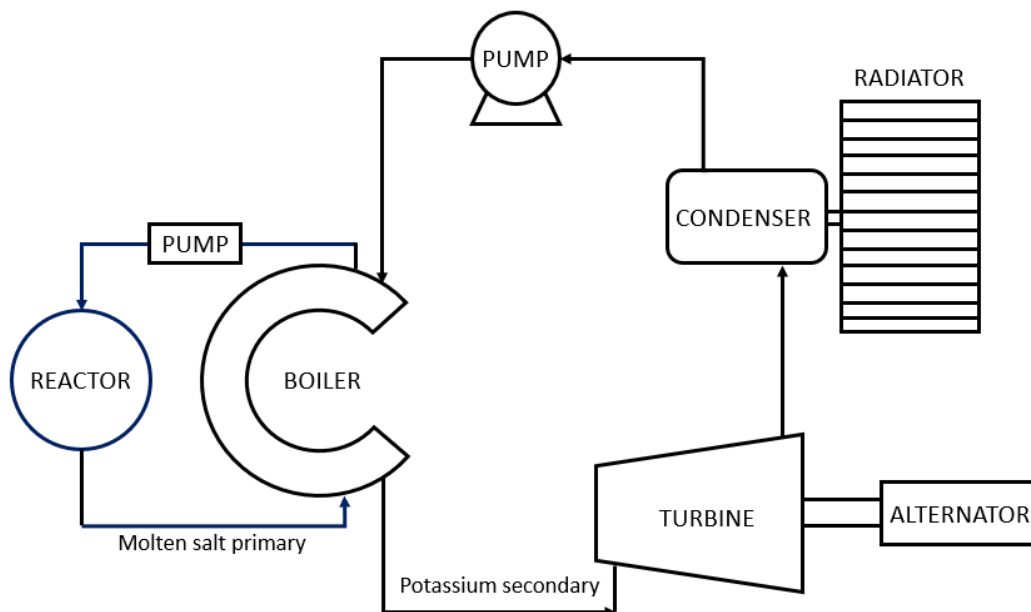


Figure 2.2: Rankine cycle schematic.

## Boiler

The boiler for an advanced Rankine cycle system must be able to produce dry and superheated vapor, it must withstand system and environmental stresses for several years, and it must be as compact as possible. Conventional stationary power plants usually make no attempt at vaporizing all the working fluid, and the two-phase moisture is driven through a separator with the aim of recirculating the remaining liquid. For sake of compactness, space reactors are generally designed to get rid of this component, requiring instead a boiler configuration capable of drying the vapor. In the absence of gravity, one of the main issues is preventing liquid droplets from settling in the fluid bulk, where they are surrounded by vapor and too far from the walls to be vaporized. If not properly addressed, this phenomenon could lead to a so called boiling crisis, which causes a sudden and substantial deterioration in the efficiency of heat transfer. According to literature, the most promising solutions identified so far rely on centrifuging the liquid to the wall by means of swirl or vortex generators [30]. The first approach is mainly employed in "once-through" configuration with a swirl movement induced by tube inserts, tube coiling or a combination of both. Several types of helical flow have been tested in alkali metal boilers and in most cases they have proven to maintain liquid on the tube wall and enhance the heat transfer performance. However, these techniques always increase pressure drop and might promote flow instabilities that must be taken care of.

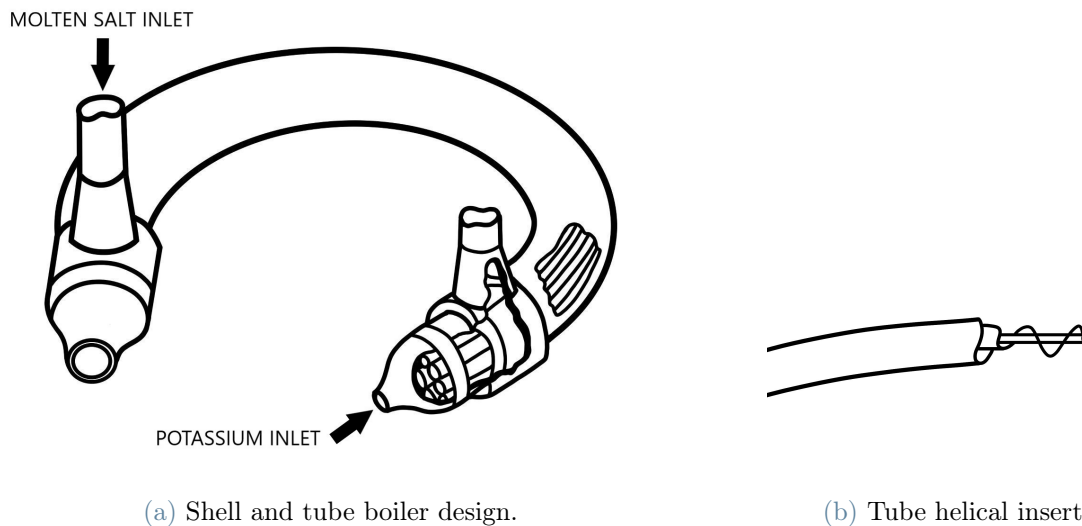


Figure 2.3: Circular-arc shaped once-through boiler with swirl generators.

The generation of a vortex flow is rather a more innovative concept. This can be achieved either by rotating the boiler or by pushing the liquid tangentially into the boiler. The

former is insensitive to gravity field and orientation, it yields a steady flow of both vapor and liquid and a low moisture content at the boiler exit, but it has the major drawback of requiring moving parts and rotating seals. The second one instead, also called cyclone boiler, does not have any mechanical part movements and aims at establishing a vortex flow pattern that drives the liquid towards the apex of the cone as the vapor exits from the opposite end (fig. 2.4) [30].

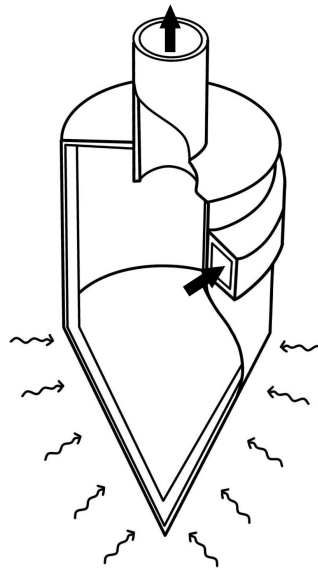


Figure 2.4: Cyclone boiler design.

Despite several advantages that make it a very promising design, the vortex generator approach was discarded in favor of a shell-and-tube boiler with helical inserts. Both the rotating and the cyclone boiler have only been tested with water and at relatively low power, whereas a larger amount of data have been collected for once-through potassium boilers [30]. Nonetheless, it is strongly believed that a lot more attention should be devoted to the vortex approach in the following years.

To obtain an exceptionally compact heat exchanger, it is a wise idea to have the largest possible heat-transfer surface per cubic meter. This implies the use of small-diameter tubes very close together, which on the other hand can lead to unacceptable stress levels and thermal expansion effects. One way of coping with these problems is actually to bend the tubes, and according to ORNL, among different configurations, the circular-arc tube bundle gives the lowest system weight [35]. The estimation of thermal-mechanical forces is a significant concern when it comes to designing a component that experiences large temperature and pressure gradients. Unfortunately, in this work, no such calculation has been performed, but some precautions are taken to keep all the analyzed configurations

very close to already tested boiler designs.

## Heat Rejection System

In the field of liquid-metal heat exchangers, the design of radiators and condensers for space applications is quite new. As already anticipated, the problem of rejecting heat in space involves several aspects that require a compromise between weight and efficiency. Moreover, the radiator is the most massive component in advanced Rankine cycles, and therefore its design must be carefully examined. At LPSC, research carried out in tandem with this thesis by Fernando Scarafia investigated different technologies such as Stirling converters, thermoelectric units and heat pipes, but after comparative analysis, the latter was found to be the best solution.

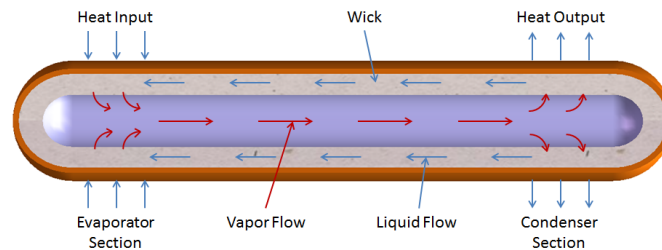


Figure 2.5: Heat pipe longitudinal section.

Invented in 1963, heat pipes (HPs) have the capability to transport thermal energy at high rates and with small temperature gradients by exploiting a pumping action exerted by surface tension forces (fig. 2.5). On the evaporator end, the external heat vaporizes the fluid and creates a pressure gradient that pushes the vapor to the cooler section. Here the vapor gives up its latent heat and condenses before being returned to the evaporator part by a capillary action generated in the wick structure. In the absence of gravity, this force must only overcome the drag of vapor through the channel, and once done, the liquid is ready to repeat the loop. These devices are very appealing for space applications: they have an extremely high thermal conductivity, and in addition, they work basically as passive systems with no need for electrical energy or moving structures. The heat rejection system is thus made by a set of heat pipes in series, with the HPs evaporator surface placed inside the potassium pipeline that comes from the turbine outlet. The condenser end is equipped with radiator fins that disperse the heat through radiation (fig. 2.6).

For what concerns the remaining components, a variety of configurations can be observed among the various Rankine cycle designs proposed over the years. Different operative conditions, output powers and materials were investigated and not always the same device

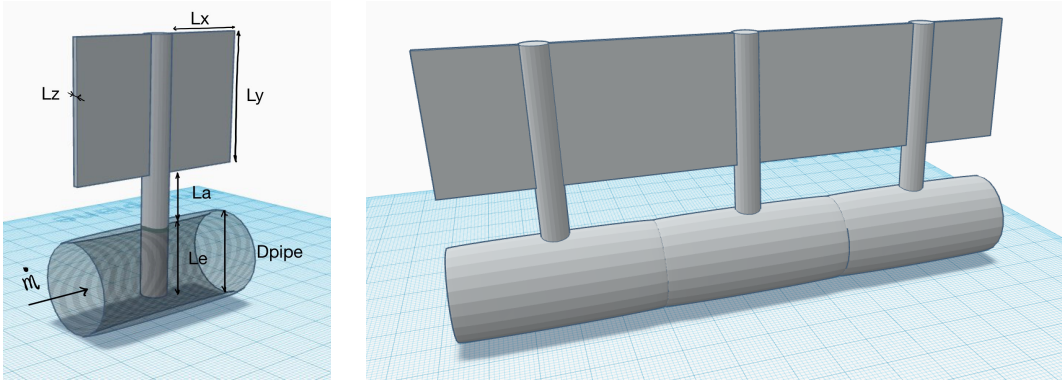


Figure 2.6: Schematic of a heat rejection system portion.

was adopted. Since we are not interested, at least with this work, in finding a component that best fits specific mission requirements, we simply adopted the technologies proposed by ORNL in one of its most recent studies [35]. In the here-mentioned report, a Rankine cycle relying on a lithium-cooled reactor is presented. Despite the different reactor concept, both the primary and secondary side operative conditions are quite close to the ones we are investigating. For this reason, similar components have been implemented in our calculations. In this section, we will limit ourselves to a short description of those devices by focusing on those features that are useful for mass estimation.

## Feed Pump

The feed pump consists of a single-stage, partial admission turbine coupled to a single-stage centrifugal pump, both enclosed in a common, canned housing without any external rotating seals. Small axial-flow turbopump performance (i.e. efficiency) and optimum operating speed can be demonstrated to be both functions of the turbine size [35]. Therefore, these two parameters should be the only ones needed for future optimization studies.

## Turbine

A nine-stage, axial flow turbine with a tilting pad bearing system lubricated with liquid potassium is used as a reference and even in this case, the turbine size is the most important parameter for system optimization. When dealing with gas turbines, other highly important quantities are the erosion effects and the moisture level in the expansion path. As the results in the next section will reveal, keeping the turbine exit quality at a sufficiently high value is probably the most challenging requirement. Potassium-turbine tests operated for thousands of hours showed negligible erosion up to 1,144 K, while a General Electric turbine test rig operated successfully with an inlet temperature of 1,088

K and an outlet vapor quality of 92% [35]. To maintain the moisture level at the turbine exit at reasonably low values, the use of external separators and interstage ones is usually advisable. Considerations of either weight penalty, efficiency and pressure load must be accounted when selecting among them, and an extensive analysis of the state of the art of these components would be needed. The adoption of one or more separators is likely to be unavoidable when the output power is increased; however, for sake of approximation, it was decided not to include any of these devices in the system or in the turbine mass calculation.

### 2.3.2. The heat transfer

Even if a heat exchanger model is already present in the *ThermoPower* library, it actually only incorporates heat transfer procedures that are suited for conventional media, mostly similar to water. However, as the underlying physical mechanisms of heat transfer to liquid metals (LMs) significantly differ from those to ordinary liquids, correlations developed for the latter are not applicable to the first [24]. The reason lies in their low Prandtl number ( $Pr$ , always below 0.05), which can be seen as the ratio of the hydrodynamic-to-thermal viscous boundary layer thickness. Therefore, for these fluids, the contribution of molecular thermal conduction to the total heat transfer is much higher than for order one and higher Prandtl number fluids. Due to this, a lot of attention has been devoted to LMs heat transfer since the 1940's and extensive information has been published in the literature, mostly under uniform-wall-heat-flux conditions. A pioneering work was made by Martinelli and Lyon [18] [19] who gave a first theoretical explanation to experimental observations, proposing an equation of the form:

$$Nu = 7.0 + 0.025\left(\frac{Pe}{Pr_t}\right)^{0.8} \quad (2.1)$$

where  $Pr_t$  is the mean turbulent Prandtl number. Afterwards, most authors proposed Nusselt number correlations based on the same functional dependence while trying to tailor the parameters to their own experimental configuration. This led to the development of a large number of heat transfer equations that are very different from each other and have been the subject of a quite recent statistical analysis by J. Pacio and L. Marocco [24]. Unfortunately, a vast majority is specifically suggested for sodium, lead, or lead alloys, which are employed, for instance, in fast reactors, in which the metals are supposed to remain liquid and never approach the boiling temperature. The latter consideration introduces a new issue with respect to those faced by common users of alkali metals in the nuclear industry: the transition to the vapor phase.

## Potassium boiling regions

Potassium boiling behavior is a phenomenon that has received very little attention and the only data we are aware of belongs to experiments performed for a very few years in the 1960's. At the Connecticut Advanced Nuclear Engineering Laboratory (CANEL) during the initial development phase of the SNAP-50 program a number of boiling potassium tests were performed to investigate and obtain basic heat transfer data. Almost 3,500 hours of test time, logged on an Haynes-25 alloy apparatus, and more than 1,200 hours on a stainless steel test loop, were used to determine the performance of various boiler tube configurations [3]. Relying on these results, a few years later engineers led by J.R. Peterson at the NASA-Lewis Research Center in Cleveland, Ohio, tried to develop empirical correlations that were derived from considerations of the flow regimes and heat transfer mechanisms [13]. Experimental outcomes suggested that four distinct heat transfer regions can be identified in once-through potassium boilers. The subcooled liquid region is defined as the region from the potassium inlet to the saturation point where boiling initiates. Once the first bubbles detach from the metal surface, the nucleate boiling region begins and extends until the local vapor quality and the heat flux become high enough such that only partial wetting of the tube occurs. The region of partial wetting is defined as the transition boiling section, and the point separating this region from the previous one is defined as the critical heat flux point. The last one is the superheated vapor region, which goes from the 100% vapor quality point to the potassium boiler exit. Eventually, a film boiling region can be encountered anywhere along the tube if the wall-to-potassium temperature difference is high enough to match the so called Leidenfrost condition but this region was neglected in this study since it was never observed in the experiments we are using as references.

For each of the four above mentioned regions J.R.Peterson proposed a heat transfer correlation best fitting the data from Rankine cycle potassium boilers tests [13]. The Dittus-Boelter equation was found to correctly estimate the heat transfer coefficient in the superheated vapor region and just a multiplier term was added to account for the vortex effect that an internal insert might produce.

$$h_{SV} = h_{DB} \left[ \left( \frac{L_H}{L} \right)^{0.8} \left( \frac{D_i}{D_e} \right)^{0.2} \right] \quad (2.2)$$

Here  $\frac{L_H}{L}$  is the ratio of helical length to axial one, while  $D_i$  and  $D_e$  are the inside diameter of the boiler tube and the equivalent diameter for the helical flow, respectively. For the subcooled liquid region the following correlation developed by Lubarsky and Kaufman

was suggested.

$$\frac{h_{SL}D_e}{k_{SL}} = 0.625(Pe)^{0.4} \quad (2.3)$$

For what concerns the nucleate boiling and transition boiling regions, after about sixty years, the relations proposed by the author are no longer available to us, and alternative or more recent correlations were not found in the literature. Thus, we decided to derive equations able to replicate at least the local potassium heat transfer coefficient trend along with the boiler length. To do that, we looked for heat transfer coefficient data coming from experimental results and from predictive code outcomes and we interpolated them. Here below, the main data sets used for calculations are reported. fig. 2.7 shows the heat transfer coefficient distribution obtained using a computer program based on the correlations proposed by J.R. Peterson and applied to a 3.3 MW example counterflow boiler, design for the Nuclear System Programs (NSP) [13]. Below that, in table 2.2, the ranges of applicability of the correlations have been reported. Whereas in fig. 2.8 the outcomes of a two phase potassium test performed during the SNAP-50 program by Pratt & Whitney Aircraft are reported, along with the test conditions listed in table 2.3 [3].

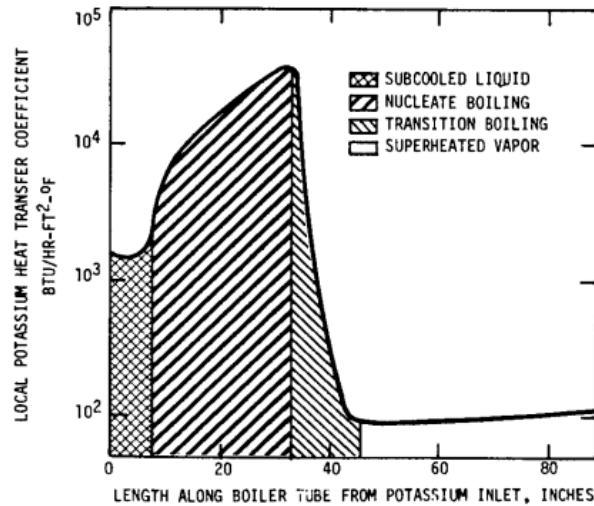


Figure 2.7: Typical distribution of heat transfer coefficient in a Potassium heated counterflow boiler tube [13].

In this way, two equations were developed, one for each region, in which the heat transfer coefficient depends only on the local vapor quality  $x$ . Since no equation for critical heat flux was available, the initiating point for transition boiling was set to a guessed value of 70% vapor quality. The CHF position also coincides with the position in which the potassium fluid reaches its highest heat transfer capability (i.e., its highest heat transfer



Variable	Range	Units
Wall-to-Potassium temperature difference	287-390	K
Saturation Temperature	1,088-1,420	k
Tube internal diameter	1.07-2.34	cm
Heat flux	157,000-790,000	W/m <sup>2</sup>

Table 2.2: Applicability ranges of the correlations implemented in the computer program used to obtain the heat transfer coefficient distribution of fig. 2.7.

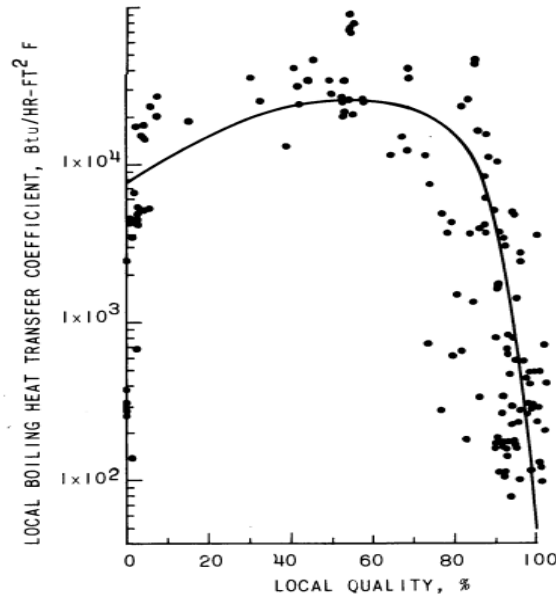


Figure 2.8: Two phase local heat transfer coefficient of Potassium obtained through a serpentine-boiler experiment carried out by Pratt & Whitney Aircraft in 1964 [3].

Variable	Range	Units
Vapor pressure	3-4.3 · 10 <sup>5</sup>	bar
Saturation temperature	1,160-1,210	K
Potassium flow rate	2.14-3.15	g/s
Heat flux	53,000-164,000	W/m <sup>2</sup>

Table 2.3: Range of experimental test conditions of fig. 2.8.

coefficient  $h_{max}$ ). For the nucleate boiling region, an equation that tied the subcooled liquid heat transfer coefficient  $h_{bubble}$  at the dew point to the  $h_{max}$  was defined as follows:

$$h_{NB} = 1.126(h_{max} - h_{dew})x^{\frac{1}{3}} + h_{dew} \quad (2.4)$$

For the transition boiling region an equation connecting the  $h_{max}$  at the point of critical

heat flux to the superheated vapor heat transfer coefficient  $h_{bubble}$  at the bubble point was calculated as:

$$h_{FB} = 0.0897(h_{max} - h_{dew})\frac{1}{x^7} + [h_{dew} - 0.0897(h_{max} - h_{dew})] \quad (2.5)$$

Once implemented, the model was tested using the input specifications of the 3.3 MW boiler mentioned above and a tentative value  $h_{max} = 1.2 \cdot 10^5 \text{ W/m}^2 \text{ K}$  was adopted to get the distribution displayed in fig. 2.9.

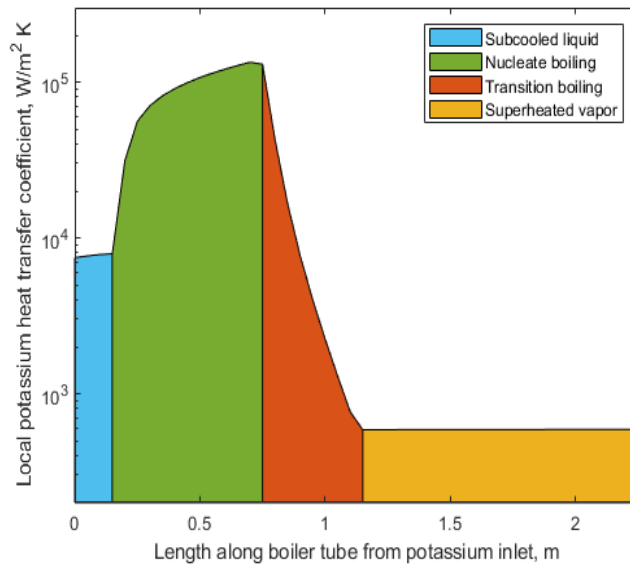


Figure 2.9: Heat transfer coefficient distribution of a 3.3 MW boiler design implemented in Modelica.

Unfortunately, it is not known how  $h_{max}$  varies with different boiler configurations or operating conditions and there is no evidence that the heat transfer behavior is not going to change with them. However, by restricting our design options within the range of applicability listed in table 2.3, the heat transfer phenomenon is expected to not drastically depart from this trend. This is for sure an approximation but it won't affect our mass estimation work too much, as will be found out once the primary side heat transfer model is introduced.

When implemented, the heat exchanger model must be tested before being used. Up to now only the potassium secondary side has been discussed but since it is the intention of this work to validate the entire boiler model, also the primary side fluid must be investigated. The validation process is expected to replicate heat exchanger designs that have already undergone testing. While no studies have yet been carried out with molten

salts, a few space researchers have employed liquid lithium for their experiments. A necessary step is thus to create models for both of these fluids to be implemented into the code and used for validation.

### Lithium heat transfer model

A vast majority of the potassium Rankine cycle conceived in the 60's for nuclear applications relies on lithium as reactor coolant and primary side working fluid. These designs were then selected to verify the goodness of the boiler model. Due to the fact that in the PCS the liquid lithium is not going through relevant state changes except for a decrease in temperature along the boiler, which is rarely higher than 50 K, its thermal-mechanical properties remain virtually the same. For this reason, only thermal conductivity and dynamic viscosity were defined as functions of temperature, while all the other properties were kept constant as described in appendix B. To calculate the heat transfer coefficient, the prediction recommended by Dwyer and Maresca was adopted as follows:

$$\frac{h_{Li} D_{eq}}{k_{Li}} = 6.66 + 3.12x + 1.184x^2 + 0.0155(EPe)^{0.86} \quad (2.6)$$

This equation has been derived after experiments in which the working fluid was Mercury ( $Pr = 0.02$ ) and it was suggested for configurations employing tube bundles with a Péclet number  $Pe$  ranging between  $70 - 10^4$  and a pitch-to-diameter ratio  $x$  between 1.3-3. As a first approximation the ratio of the eddy diffusivity of heat to the one of momentum,  $E$ , was assumed equal to unity.

### Molten salt heat transfer model

Thanks to the different applications of molten salts as engineering fluids, research activities involving a variety of salt formulations have been carried out in the last decades. The reactor design under investigation at LPSC is meant to be operated using LiF-UF<sub>4</sub> with enriched Lithium-7 to improve core neutronic performance and a melting point of 760 K. To evaluate the non-dimensional parameters which in turn allow to estimate the heat transfer behavior, it was made the simplifying choice to consider the molten salt properties as constant and equal to those values computed at 1,150 K, as shown in table 2.4.

Despite some slight differences among the various salt mixtures, the Prandtl number usually decreases with temperature by about one order of magnitude but never goes below unity. The heat transfer correlations adopted above for lithium are thus incompatible with molten salts and more suitable equations were sought. After a review of several experimental results for forced convection involving molten salt no data were found for

Variable	Value
Density ( $\rho$ )	4453 kg/m <sup>3</sup>
Specific heat capacity ( $Cp$ )	1065 m <sup>2</sup> /s <sup>2</sup> K
Thermal conductivity ( $k$ )	1.02456 W/mK
Kinematic viscosity ( $\mu/\rho$ )	8.61 · 10 <sup>-7</sup> m <sup>2</sup> /s

Table 2.4: LiF-UF<sub>4</sub> properties kept constant in the model.

LiF-UF<sub>4</sub>, nonetheless, several studies focused on the fluoride eutectic LiF-BeF<sub>2</sub>-ThF<sub>4</sub>-UF<sub>4</sub> which is also advised for molten salt breeder reactors. For the latter, correlations from Sieder-Tate were found to adequately predict experimental measurements in a turbulent regime, whereas the Hausen equation showed better agreement for a transitional one [17]. A more recent study also compared the outcomes of heat transfer experiments using molten LiNO<sub>3</sub> with the predictions from Dittus-Boelter, finding a discrepancy as high as 25%. Regardless of this evidence, we preferred not to develop a new heat transfer model for the primary side, using instead the already implemented one based on the mentioned Dittus-Boelter correlation. By the way, it is believed that, for a higher accuracy level, those equations reported in Table 2.4 should rather be considered.

Author	Equation	Validity
Sieder and Tate	$Nu = 0.027(\mu_b/\mu_w)^{0.14} Re^{0.8} Pr^{1/3}$	$0.7 \leq Pr \leq 16,700$ $Re > 10,000t/d > 60$
Hausen	$Nu = 0.037(Re^{0.75} - 180)Pr^{0.42}[1 + (d/l)^{2/3}](\mu_b/\mu_w)^{0.14}$	$2,300 \leq Re \leq 10^6$ $0.6 \leq Pr \leq 1,000$

Table 2.5: Forced convection correlations for flow in circular pipes.

## The overall heat transfer

For a proper design, the two sides of a heat exchanger cannot be considered separately and a coupled analysis is mandatory to point out the different heat resistances. Therefore, through the calculation of the overall heat transfer coefficient, we want to better understand how the heat flux varies along the boiler. In fact, since our main interest is in mass reduction, techniques to enhance heat transfer can be adopted in those regions requiring the largest heat transfer area. Using once again the specifications of the NSP cycle system, we computed the overall coefficient, including the heat conduction effect across the tube walls, using Nb-1%Zr as the design material.

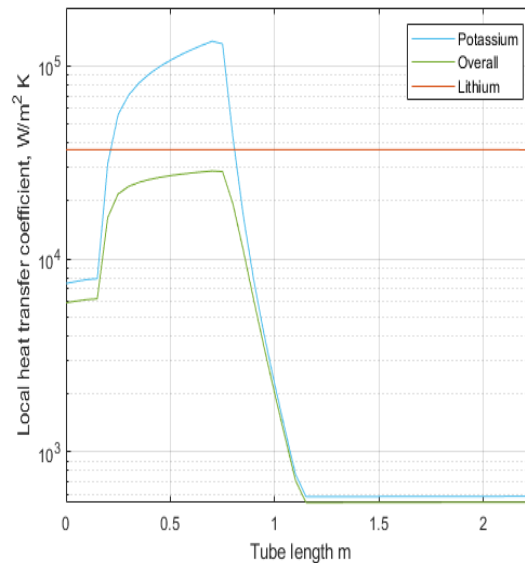


Figure 2.10: Overall heat transfer coefficient distribution for a 3.3 MW Nb-1%Zr boiler design with lithium at the shell side and potassium at the tube side [13].

As can be seen from fig. 2.10 potassium heat transfer coefficient is not the determining factor throughout most of the low-to-medium quality region since the lithium-side coefficient sets the required exchange area in that region. Due to the worse heat transfer capability of the molten salts, this effect would be even more pronounced in our design. As the quality raises the tube wall becomes dry while liquid droplets are still present in the stream and this makes the potassium coefficient fall to the gas value. This coefficient plays a major role in sizing the remainder of the boiler and to mitigate its effect, it is desired to postpone the shift to transition boiling to a quality as high as possible, in order to minimize the amount of heat to be transferred within this region. To accomplish it the SNAP-50 boiler design proved the effectiveness of a twisted tape insertion in the tube. Producing a force field, these inserts tend to centrifuge liquid droplets to the outer wall where they can be directly vaporized. The resulting effect is that of raising the dry-wall transition point from a quality of about 50% to one of 80-90%. This coefficient improvement can represent a substantial saving in boiler size, which means a reduction in system weight. Delaying the onset of the critical heat flux condition gives also some benefits from an experimental point of view. It does indeed set a different level of accuracy for the knowledge of various coefficients, shifting the focus from the hardly-measurable boiling region to the primary side and high-quality secondary side. Although these results seem very promising, the conservative choice to not move from the 70% vapor quality for the CHF point was made.

As told, swirl-generating inserts primarily affect the heat transfer in the boiling region but according to J.R. Peterson, a non-negligible impact can be appreciated also in the superheated one [13]. To account for that, an approximate enhancing multiplier  $\gamma_{insert}$  that ranges between 1.5 and 2.5, depending on the insert geometry, was calculated after the eq. (2.2) proposed by the author itself.

$$h_{insert} = h_{SV} \cdot \gamma_{insert} \quad (2.7)$$

Eventually, as already underlined, helical inserts also help in promoting wall wetting in the space environment where no buoyancy force is present at the expense of increased working fluid pressure drop.

### 2.3.3. Boiler model validation

Once implemented, the heat exchanger model must be tested before being used. Since new models were introduced both for the working fluid properties and the heat transfer coefficient calculation, a validation is advisable to verify the predictive capability of the code as well as its reliability. To do that, we referred to boiler studies carried out several years ago as benchmarks to perform some code assessment. Even though some of those works have already been mentioned above, a more detailed presentation of all the design specifications is provided here.

The first study pertains to a 300 kWe advanced Rankine-cycle space-power system designed by a research team at Lewis Research Center in Cleveland, Ohio [15]. It's a work that dates to 1969 and was sponsored by NASA. This prototype was based on the use of a 2 MWth fast-spectrum nuclear reactor cooled by a lithium loop able to transfer heat from the reactor to the shell-and-tube boiler. Hereafter, the potassium working fluid is heated up to superheated vapor condition and enters a multistage axial-flow turbine, which directly drives an electrical generator. To produce relatively dry potassium vapor at 1,420 K at the boiler exit, flowing lithium must enter at 1,480 K. To do that, General Electric prepared a once-through boiler design that consists of 31 tubes, each 230 cm long and 0.076 cm thick, containing swirl generators and accommodated within a 15.2 cm diameter shell. Since the diameter of the tubes is in the range of 1.27 to 1.9 cm, an average value of 1.6 cm was chosen as the Modelica input value. Lithium and potassium flow countercurrently and both the tubes and shell have been formed into an arc of a circle and are meant to be constructed using the refractory-metal alloy T-111.

These design features, summarized in table 2.6, were implemented into the Modelica code, keeping the same heat transfer assumptions mentioned in the section before. In this way,

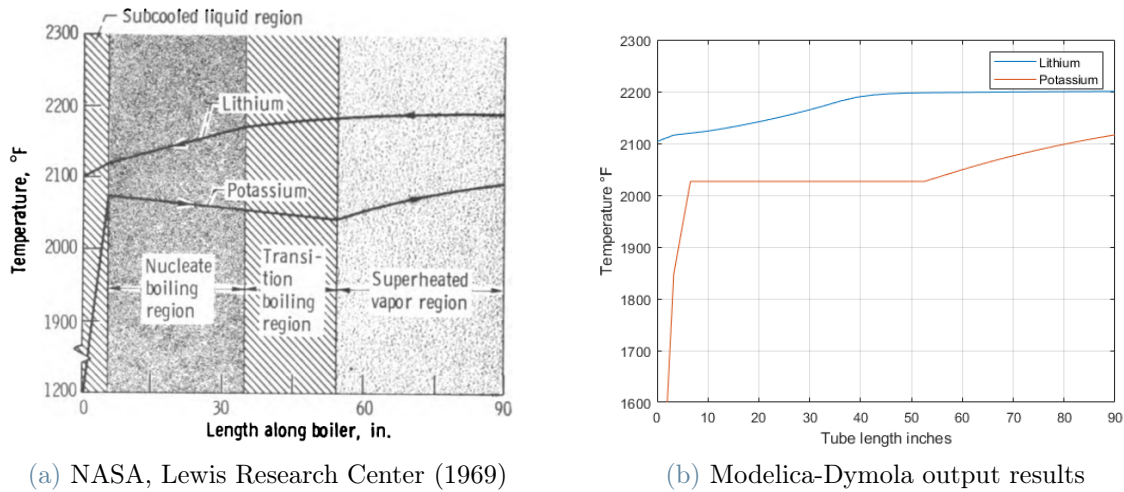


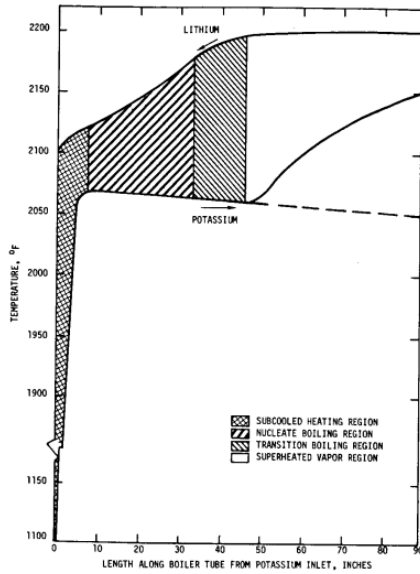
Figure 2.11: Comparison of temperature distribution in a 2 MWth once-through potassium boiler design for advance Rankine space-power system [15].

the temperature distribution shown in fig. 2.11b was obtained and compared to the one reported by the authors reported in fig. 2.11a. The result obtained matches quite perfectly, except for a slight overestimation of about 20 K at the potassium-side boiler outlet. A possible explanation could be found in the absence of pressure losses along the heat exchanger. Different correlations are actually available within the *ThermoPower* library but none of them specifically accounts for tube inserts. As it can be seen, a pressure decrease has the effect of lowering the saturation temperature value. On the other side, this can be a benefit for the heat transfer in the high-quality region since there is a gain in the difference in temperature with the primary fluid. After all, to not overwhelm computer calculations, pressure drops have been neglected in this component.

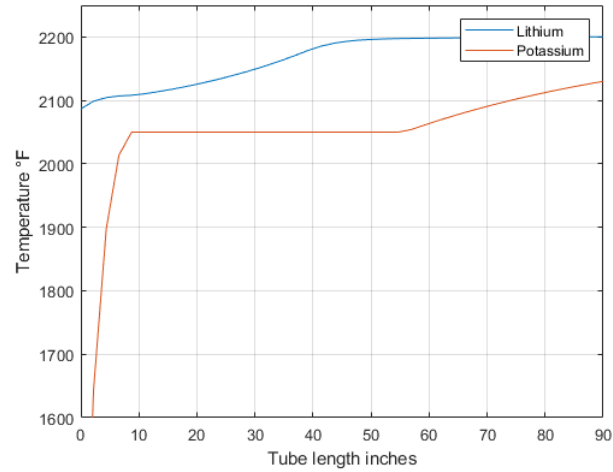
	Parameters	Values
Lithium	Inlet temperature [K]	1,480
	Pressure [Pa]	$10^5$
	Mass flow rate [kg/s]	8.70
Potassium	Inlet temperature [K]	929
	Pressure [Pa]	$11.3 \cdot 10^5$
	Mass flow rate [kg/s]	0.94

Table 2.6: Design specifics for a 2 MWth once-through potassium boiler developed by NASA in 1969 [15].

A second test was made through a comparison with the output results obtained thanks to



(a) Nuclear Systems Programs, 1968.



(b) Modelica-Dymola output results.

Figure 2.12: Comparison of temperature distribution in a 3 MWth once-through example boiler design [13].

a computer program developed by the already mentioned J.R. Peterson's research team. As part of the Nuclear Systems Programs, the author presented a procedure on how to properly design a boiler for advanced Rankine cycle space power systems [13]. Once implemented as a code, the procedure was used to predict the length of a single tube in a once-through mercury boiler, showing a discrepancy within 15%. It was then applied to an example heat exchanger with a countercurrent flow configuration. The latter, an arc shaped boiler with fifty-five 1.9 cm external diameter tubes and a 23.6 cm diameter shell, was supposed to transfer 3.3 MW of heat from lithium flowing at 13.15 kg/s to 1.6 kg/s of potassium. Helical inserts were present in this design as well. After the optimization calculation, a total boiler length of 226 cm yielded the minimum mass for the system. Once again, all the input specifications reported in table 2.7 were used for the Modelica model. A good agreement for the potassium-side is attested to by results in fig. 2.12 and a not so worrying 14% higher difference of temperature between the lithium inlet and outlet is predicted.

These validation processes demonstrate the goodness of the heat exchanger model for a limited range of operative conditions. Unfortunately, no more benchmarks were available to us, so the optimization was conducted, taking into consideration that a certain level of uncertainty can be attributed to this part when exceeding those limits.



	Parameters	Values
Lithium	Inlet temperature [K]	1,480
	Pressure [Pa]	$10^5$
	Mass flow rate [kg/s]	13.15
Potassium	Inlet temperature [K]	866
	Pressure [Pa]	$12.08 \cdot 10^5$
	Mass flow rate [kg/s]	1.60

Table 2.7: Design specifics for a 3 MWth once-through boiler developed by J.R Peterson in 1968 [13].

## 2.4. Mass estimation

Since the very beginning, the purpose of this work has been to find how the system mass was affected by any design change. To do that, a mass estimation of each component is performed using equations that have been implemented in the Modelica code in order to get specific results for each configuration that was tested and simulated.

### Boiler

To evaluate the heat exchanger mass, a simple and approximate geometrical calculation is employed. Having as input values the internal diameter of each boiler tube, their thickness and length the tubes-side volume is calculated, and likewise for the shell side. Once the appropriate construction material (i.e., one with a certain density value) was selected, the mass estimation is quite straightforward. In doing so, we also considered an extra mass of about 20% of the tubes to account for swirl-generators, wire spacers between tubes and the single inlet and outlet tube. The shell can be equally designed to have a toroidal shape as well as a circular-arc with a rectangular section. As it often happens for operations involving high temperatures and large gradients, the employed material establishes the working limits. However, not only should considerations about strength or corrosion resistance be made but also ones about manufacturing and costs. At last, an evaluation of the molten salt and potassium inventory masses is included in the calculation.

### Heat Rejection System

A similar geometrical estimation is performed for the heat rejection system. Internal diameter, wick thickness, evaporator, adiabatic and condenser lengths of the heat pipes

are optimized with constrains imposed by the sonic, the entrainment and the wicking limit. Considerations of the heat-rejection surface over mass drive the radiator design, while also taking into account some safety margins for the reliability of this component, which is completely exposed to the external space environment [34]. Several materials were tested for the heat pipe and even though some of them showed better performance, the choice of Nb1%-Zr is mainly dictated by corrosion prevention. This phenomenon is governed by the potential difference between metals and to avoid the possibility of having different materials dragged by the potassium flow along the circuit, it's better to employ similar metals in the whole primary loop. Moreover, this might have some benefits from the component crafting and welding standpoint. Potassium is selected as the working fluid for the heat pipes, whereas the radiator plates are in carbon-carbon (C-C), a composite material that is well known in the spacecraft industry since it was widely used for the nose cone and wing edges of Space Shuttles. In conclusion, the optimization process provides two equations relating the total mass of the heat rejection system  $M_{HRS}$  to a couple of variables: the amount of heat that the system is required to reject ( $Q_{rej}$  in Watts) and the temperature at the turbine exit ( $T_{out}$  in Kelvin).

$$M_{HRS} = \gamma_{HRS} \cdot Q_{rej} \quad (2.8)$$

$$\gamma_{HRS} = 1.185 \cdot 10^{22} \cdot T_{out}^{-8.554} \quad (2.9)$$

These correlations, presented in fig. 2.13, are included in the overall mass estimation and since the temperature at the turbine exit (i.e., its outlet pressure) influences the system performance, the optimal combination is found at the end of the optimization procedure.

## Feed pump and turbine

For both the feed pump and the turbine, the mass scaling expressions proposed by ORNL are employed as follows [35]:

$$M_{pump} = 10 \cdot (5252 \cdot \frac{P_{hyd}}{N_{pump}})^{0.6} \quad (2.10)$$

$$P_{hyd} = 1.34 \cdot 10^{-3} \cdot G \frac{\Delta P}{\rho} \quad (2.11)$$

where

$$M_{pump} = \text{feed pump mass (kg)}$$

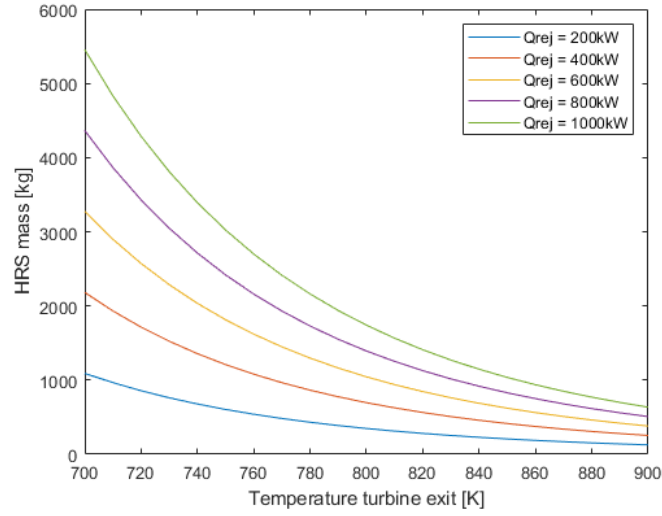


Figure 2.13: Heat rejection system mass scaling as function of turbine exit temperature with different heat loads to be rejected.

$N_{pump}$  = turbine speed (rpm)

$P_{hyd}$  = pump hydraulic power

$G$  = pump drive flow rate (kg/s)

$\Delta P$  = pump pressure rise (Pa)

$\rho$  = local pumped fluid density (kg/m<sup>3</sup>)

$$M_{turb} = 646 \cdot \left( \frac{P_m}{N_{turb}} \right)^{0.6} \quad (2.12)$$

where

$M_{turb}$  = turbine mass (kg)

$N_{turb}$  = turbine speed (rpm)

$P_m$  = turbine shaft power (kW)

Even if these relationships do not define a pump and turbine design, they provide sufficient information to get a rough mass estimation and to eventually proceed with system optimization.

## Other components

To get an extensive comprehension of the power conversion system, those devices not directly implemented into the computer tool are also partially considered in the mass computation. The generator, the alternator and the power management and distribution (PMAD) system were not included in the model mainly because they have no impact on the physics of the Rankine cycle. Despite that, they are of paramount importance if one wants to control the system and produce any electricity out of it. A dedicated study about these units is out of the scope of this work but once again to account for their mass variation along with the changes in system specifications, expressions suggested by researchers at Oak Ridge were adopted [35]. As an alternator, a homopolar inductor type is suggested; despite its somewhat low efficiency compared to other machines, it can operate at high temperatures and perform in adverse environments. Its mass (kg) is estimated using the following relationship:

$$M_{alternator} = 26300 \cdot \frac{P_e}{pf \cdot N} \quad (2.13)$$

where  $N$  is the operating speed and  $\frac{P_e}{pf}$  is the alternator complex power (kVA) derived from the electric power  $P_e$  using a power factor  $pf = 0.85$ . The PMAD system is responsible, among others, for the distribution of the power produced by the turbo-alternator to the payload area. It also contributes to delivering conditioned power to the thruster propulsion units and spacecraft. A PMAD configuration with one channel working and a second one that is redundant is selected and the corresponding mass equation, a function of the total thruster power  $P$  (kW), is applied as follows:

$$M_{PMAD} = 463 \cdot \left(\frac{P}{100}\right)^{0.691} + \left(\frac{P}{160}\right)^{7.68} \quad (2.14)$$

Cabling, power system controller, MUX, sensor, reflector stepper motors and stepper motor drives are all units required to control and monitor power system operation. These are included into an instrumentation and control (I&C) subsystem and their mass (kg) is estimated as:

$$M_{I\&C} = 129 \cdot \left(\frac{P}{100}\right)^{0.26} \quad (2.15)$$

During launch, ascent and as long as the spacecraft has not reached the so-called nuclear safe trajectory, the reactor won't receive the start-up signal. In the meantime, several

control systems are still supposed to be operational and solar array and battery would supply them with the required power. Those devices and all the related electronic parts belong to the Auxiliary Power Subsystem (APS), whose mass (kg) is evaluated as:

$$M_{APS} = 112 \cdot \left(\frac{P}{100}\right)^{0.44} \quad (2.16)$$

Power limitations ranging from 100 kWe to 300 kWe were indicated by the authors for the applicability of the equations calculated for PMAD, Instrumentation and Control and Auxiliary Power systems [35]. For the sake of the system optimization they were included only in a successive analysis, neglecting their presence for those calculations involving power levels out of their range. On the other way no instruction were given for turbo-generator, alternator and feed pump correlations and so a preventive evaluation of their behaviour at power different from the nominal 100 kWe of the ORNL design was made.

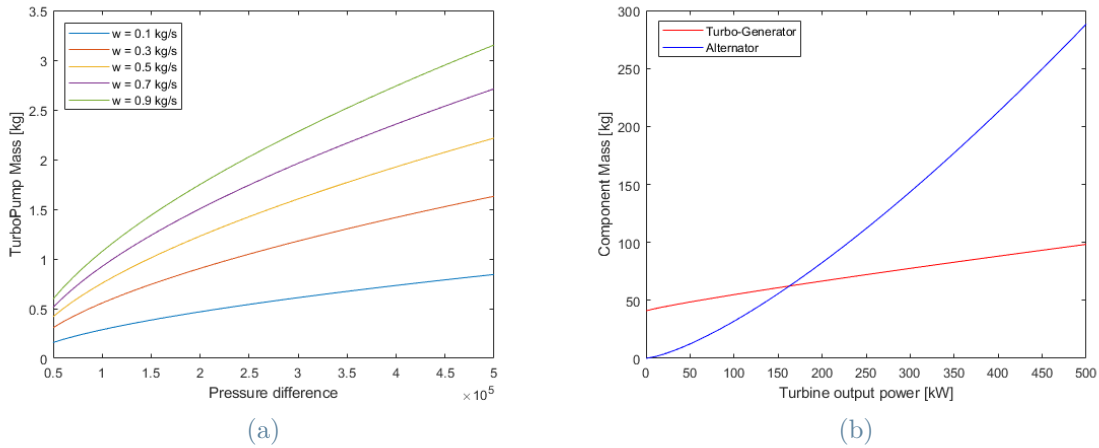


Figure 2.14: Mass scaling of feed pump (a), turbo-generator and alternator (b).

Feed-pump mass dependence on pressure rise and mass flow rate calculated at a velocity level of 24,000 rpm are displayed in fig. 2.14a. In the same way, the increase in mass of turbo-pump and alternator is presented in fig. 2.14b as a function of the output turbine power. In both cases, the mass scales following expected trends for such types of components, so their inclusion in the mass estimation for different power levels was not disputed.

At the end of the day, the total mass estimation will likely be incorrect. When it comes to the design phase, maybe more components will be required and a different configuration will be adopted, however, this is not important. For this optimization procedure, the key

aspect is to define the component weights in terms of functional dependence rather than their absolute value. This should help define the bigger picture and the starting point for the successive design process.

# 3 | System optimization

## 3.1. Optimization procedure

In the previous chapter, all the arrangements needed in our Modelica framework were addressed and discussed. The implemented Rankine cycle model plays a key role within the overall optimization procedure and we could say it represents its beating heart. In fact, all the calculations related to mass, energy and momentum balance as well as those for the system mass estimation are incorporated in the computer code. However, Modelica is not a tool intended to perform optimization on any component design. This implies that, for instance, all the required geometric quantities that can influence the heat transfer and, in turn, the boiler mass estimation as the tubes diameters, etc., must be given as input values and the same goes for the turbine. Thus, it is not possible to fix a desired power level and expect the tool to accord all the other variables. Because of that, multiple simulations with several input values hence different cycle configurations had to be run. In this way, it is possible to create a metamodel composed of a large database of Modelica output values such as the power, the superheating level, the turbine outlet quality, etc., each one associated with a specific Rankine design. Once refined, the metamodel is transferred to an appropriate numerical environment, where the actual optimization is performed. The declaration of desired constraints is the last step needed to start the numerical computation, which eventually provides the combination of variables (i.e., Modelica inputs) yielding the best result for the optimized quantity.

### 3.1.1. Modelica Rankine cycle model

The creation of a database is fundamental to gather all the results of the thermodynamic simulations and to analyze them in an efficient way. At the beginning, the database is nothing but an empty box and to fill it, combinations of input and output values must be assigned to each row of its matrix structure. For this Rankine cycle study, the inputs can be operative conditions, geometrical configurations, etc., whereas component masses, power and so on represent the outputs. To compute these quantities, several differential

and linear equations must be calculated together, employing numerical and mathematical methods as well as trial and error procedures. After having set the desired input parameters, Modelica is capable of handling these calculations and eventually providing some desired outputs. The implementation of a computational model that simulates a Rankine cycle and its annex physical laws has been the first stage of this work. In the primary loop, only three components are included: a source of mass flow rate with a fixed inlet temperature, a tube-like unit to reproduce the geometrical configuration of the boiler shell side and a sink to impose a specific internal pressure. The secondary loop unfolds in the opposite direction in order to generate a counter-current flow on the boiler tube side. This part is probably the most delicate from the computational point of view since a trial-and-error method must be used to handle counterflow equations. Precise initial values must be assigned to the solver for the inlet temperatures of both sides as well as the average bulk temperature of the metal tube. Especially when thermal power is increased and the spatial volumes that discretize the boiler length experience large variations in temperature between each other, non-convergence issues might appear.

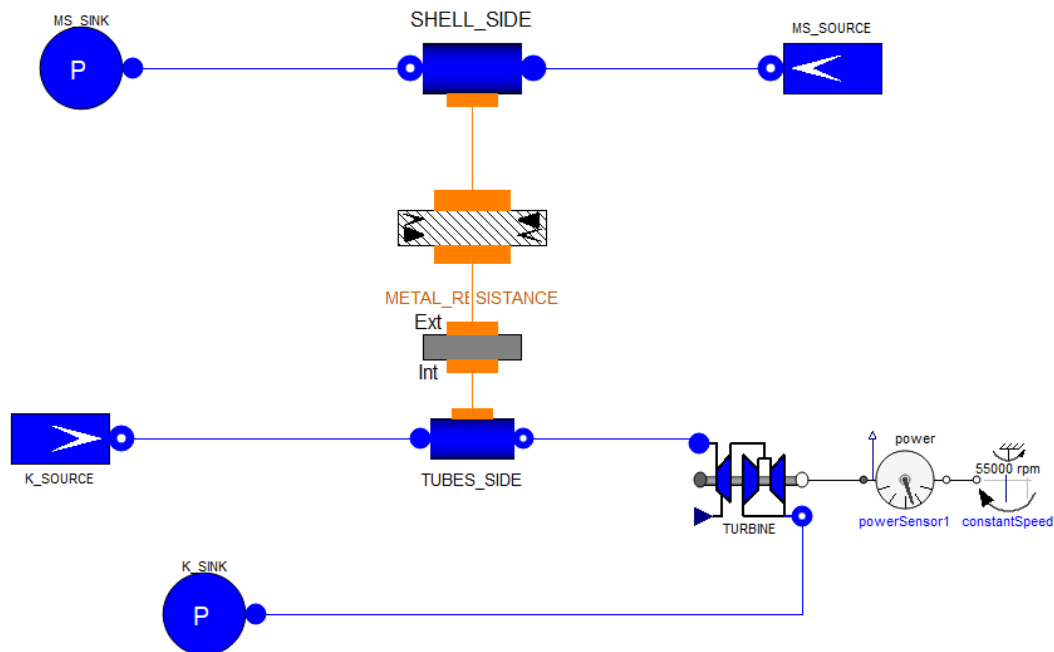


Figure 3.1: Rankine cycle layout in the Modelica environment.

In addition to the already mentioned components, the potassium circuit also adds a single-stage turbine with an input pressure value at the inlet, a fixed rotating speed and both the mechanical and isentropic efficiencies to be indicated in advance. As part of the heat-exchanger, a cylindrical-tube part accounts for the effect of heat conduction through



a metal thickness, with all the material properties being input quantities. To conclude the setup of the heat transfer section, also the exchange surfaces of both sides are input values: the cross section of the flow, perimeter of heat transfer, and the number and length of the tubes must be declared a priori. The resulting schematic of the cycle as it appears within the Modelica interface is presented in fig. 3.1 while a brief description of each component model is given in table 3.1. For a more detailed overview, always refer to appendix C.1.7.

### 3.1.2. Variable to optimize

The need for a power conversion system as light and compact as possible forces attention to the mass as the prominent parameter to allow a comparison between different designs. However, the overall system mass is a meaningless quantity if an analysis between units operating at distinct power levels is of interest. Several power sources can be investigated for electric propulsion applications, as well as multiple reactor concepts. In addition, the same reactor can be operated at a power level that is not the highest possible if this choice implies a better efficiency or a worse weight penalty. For instance, the thermal power extracted from the molten salt side could be regulated by adjusting the pumping power (i.e., the molten salt flow rate), with a consequent change in the temperature difference of the fuel between the inlet and outlet. All in all, a more useful system quantity is the specific mass, defined as the ratio between the overall PCS mass and the thermal power exchanged in the boiler or the electric power produced by the generator. This parameter is probably best known for its inverse quantity, the specific power or power-to-weight ratio, which is paramount for all those fields in which the performance of an engine or power source is studied, whether for terrestrial or space vehicles.

The Rankine model developed along with this work includes devices that ensure the conversion of mechanical power generated by the turbine into electric one and its distribution to payload and thruster units. Although these operations usually have a relatively high efficiency (above 85%), part of the power produced by expansion in the turbine is lost before reaching the propulsion units. Nonetheless, the assumption of an ideal conversion process was made without accounting for any efficiency calculations. This approximation allowed for easy computation of the specific mass by using the mechanical power produced by the turbine as an electric output.





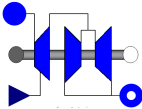
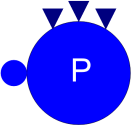
Component picture	Component description
	<p><b>Source Mass Flow</b> sets a flow rate and an initial temperature or enthalpy to the fluid.</p>
	<p><b>Flow-1DFV-2ph</b> is a one-dimensional fluid flow model for either one-phase or two-phase mixture. The mass, momentum, and energy balance equation are discretized with the finite volume method.</p>
	<p><b>Metal-Tube-FV</b> is the model of a cylindrical tube of solid material with the heat capacity lumped at the center of the tube thickness.</p>
	<p><b>Counter-Current-FV</b> is used to model counter-current heat transfer.</p>
	<p><b>Steam-Turbine-Unit</b> describes a simplified steam turbine unit.</p>
	<p><b>Sink-Pressure</b> is a pressure sink for fluid flow.</p>

Table 3.1: Rankine cycle component models in Modelica

## Parameters, variables and constraints

Since the aim of this work is to define an optimization procedure, multiple design configurations must be compared to find the optimal one. In fact, as it will be clarified in the following sections, the creation of the metamodel requires as much data as possible to define relationships between each variable of the model. This implies simulating the

system thousands of times and since each set of outputs corresponds to a distinct input choice, a matrix of different configurations and designs must be tested. However, not all the variables inside the model are free to undergo optimization. For instance, the primary side pressure does not affect the molten salt in any way, so a constant value of 1 bar was assigned to it. A turbine speed of 55,000 rpm is set as a fixed value since it is the one recommended by ORNL. In addition, turbine efficiencies have been set to unity for all the performed simulations. This is of course an optimistic approximation from the mechanical point of view, given that the state of the art of these compact turbines hardly overcomes an efficiency of 80%. On the other hand, even if an expansion without an increase in entropy grants a higher enthalpic jump, it also means a lower vapor quality at the turbine exit. Limiting the amount of liquid droplets inside the turbine is a big concern from an engineering standpoint and by considering the process as isentropic, we are adopting a slightly conservative measure.

A similar approach was followed for those parameters associated with the boiler material selection, such as density, thermal conductivity and the minimum thickness of tubes and shell. A comparison between different materials is out of the scope of this optimization procedure and further studies are suggested only for successive stages. Although an analysis of the employable metal alloys has been carried out, suggesting Nb-1%Zr, Cb-1%Zr and TZM as good candidates [3], the use of the former, which is the one selected by ORNL [35], is dictated by a mere matter of priority. In fact, the effect of conduction resistance is quite subtle for such good thermal-conductor metals and for very thin tubes, moreover, the boiler is one of the lightest components and a change of density is not going to significantly affect the overall mass. Nonetheless, material choice is way more important for aspects related to mechanical resistance, thermal expansion, corrosion effects and compatibility with the extreme space environment. To summarize, this kind of advanced heat exchanger is a very delicate component that must be able to withstand severe conditions and for instance, the possibility of a failure is one of the reasons that led the ORNL research group to opt for a redundant unit. Since considerations of this genre haven't been addressed within this work, the decision to refer to the metal adopted at Oak Ridge is made. In particular for Nb-1%Zr a tube thickness of at least 0.8 mm and a shell thickness of 1.2 mm are suggested and therefore used as inputs in the Modelica model. Before deciding to keep these values fixed for all the simulations, regardless of both the components diameter and the pressure levels, an estimation of the minimum thickness  $t_m$  for this material was performed. The design rule present in the ASME Boiler and Pressure Vessel Code for protection of a pipe against primary membrane stresses due to internal pressure loading was followed and has been reported here for sake of clarity.

$$t_m = \frac{pD_o}{2(S_m + 0.4p)} \quad (3.1)$$

The same verification for the shell side was carried out through the ASME code equation defined for a cylindrical shell.

$$t_m = \frac{pR}{(S_m - 0.5p)} \quad (3.2)$$

In both cases, an allowable stress  $S_m$  equal to 1/3 of the material tensile strength is adopted. By covering a large range of values of internal pressure  $p$ , pipe outer diameter  $D_o$  and shell radius  $R$  the equations yield lower boundaries, which are always lower than the ones adopted in this work. This might suggest that thinner pipes cannot be manufactured while still granting sufficient protection against corrosion and erosion. At the moment, an evaluation of a possible increase in pressure on the molten salt side (i.e external pressure for the tubes) due to the formation of fission gases has not yet been performed. This phenomenon is known to cause large pressure gradients in large scale reactors but its consequences in a compact version must be studied. All the parameters discussed in this section are also reported in table 3.2.

	Parameters	Values
Turbine	Speed [rpm]	55,000
	Mechanical efficiency [%]	100
	Isentropic efficiency [%]	100
Boiler	Material type	Nb-1%Zr
	Material density [kg/m <sup>3</sup> ]	8,590
	Material thermal conductivity [W/(m·K)]	50
	Primary side pressure [bar]	1
	Tube thickness [mm]	0.8
	Shell thickness [mm]	1.2

Table 3.2: List of the Rankine cycle model parameters kept fixed for all the simulations.

So far, all the parameters that remain constant in the model have been discussed, however to complete the set of inputs that are needed to define what we call a Rankine cycle configuration, a value must be assigned for any simulation also to the following variables:

- Primary side mass flow rate

- Primary side inlet temperature
- Primary side inlet pressure
- Secondary side mass flow rate
- Secondary side inlet temperature
- Total heat transfer surface

Combining several values for each of these quantities makes it possible to build a matrix of configurations to be evaluated in the Modelica framework. In principle, this process could be applied by assigning any sort of value to every mentioned variable, but this would inevitably lead to several non-physical design conditions. It's thus a pivotal part of the database definition: the selection of adequate input intervals. This procedure is usually in strong connection with another relevant optimization aspect, which is the constraint definition. The latter is not only a requirement for every numerical tool that finds the optimum of a certain function but in the case of this work is also a driver for identifying the input ranges of interest. In general, a constraint expresses a condition that the optimal variables are required to satisfy. Especially in the Python environment, it is important to carefully distinguish between the latter definition and the one of variable boundary. As it will be further explained in the next section, both constraints and boundaries are inputs for the optimizing tool, but a lower or upper boundary is just a threshold value that the variables must not overcome. Instead, a constraint is a function, different from the one to optimize but depending at least on one variable shared with the latter.

In regards to this work, constraining the mass function that has to be minimized means adding one or more requirements to the objective design system. Thus, any optimization process was done by demanding a certain power level, a minimum quality at the boiler exit and a low enough moisture level in the turbine. In principle, considering only these limits, a lot of different combinations of mass flow rate, inlet temperature, etc. could be assigned to the model; however, the PCS operational conditions cannot be defined alone without considering the power source too. In fact, the molten salt is supposed to circulate in the reactor core without ever experiencing a temperature difference between the inlet and outlet that is greater than 50 K. This safety limit is placed to keep the salt properties in a range that does not significantly affect the neutronic, thermal-hydraulic or more generally the stability of the reactor. Fixing a maximum difference of temperature between the hot and cold leg of the primary side considerably narrows the interval of values associated with a specific power level. Therefore, the attempt to cover almost all the included configurations was done by assigning three adequately chosen values to each

of the above-mentioned variables and by creating in this manner a database of inputs with all the possible combinations. Proceeding in this way, different input matrices were created for five thermal power levels, 60 kW, 120 kW, 250 kW, 1 MW and 2 MW and four primary side inlet temperatures, 1,100 K, 1,150 K, 1,200 K and 1,250 K. Although the highest power level is very far from the nominal MSR power, it was still included to broaden the range of results and improve the statistics.

A Modelica script was eventually implemented in order to perform multiple simulations using one by one the input combinations present in the database. In this way, a large amount of data is obtained, including temperature profile along the boiler, fluid-property changes in the cycle and so on, however not all of them are strictly needed for the meta-model definition and this will be better explained in the next section.

### 3.1.3. Metamodel creation

A metamodel is commonly conceived as a simplified model of another model or system. In other words, if the latter is created to describe phenomena of the real world using theoretical equations, empirical laws or other kinds of relationships, a metamodel is nothing but an abstraction of the model itself. In general, the metamodeling process involves identifying relations or properties between the components, namely the outputs and inputs of a model and expressing them through algorithms. In our case, the Rankine cycle model implemented on Modelica represents the main model, whereas the database of different design configurations and the associated output values constitutes the base for the development of its metamodel. Being a sort of macro description of the actual phenomenon, not all the variables and parameters present in the former are still employed to build its *meta* version. In short, given the system quantity that has to be optimized, some inputs might be more or less important than others and choosing to include all of them is not always worth it. To better understand this concept, it's necessary to delve into the computational issues related to the metamodeling method that is adopted within this work.

## Numerical computation

The main purpose of modeling an already existing model is to find an easy-to-handle relationship among different parts of the model. This process can be accomplished in various ways, and in this work, the numerical link between an output quantity and the inputs is established by a multi-variable linear interpolation. Within the Python environment, by exploiting the open-source software named *SciPy* and its piecewise interpolator in multi-

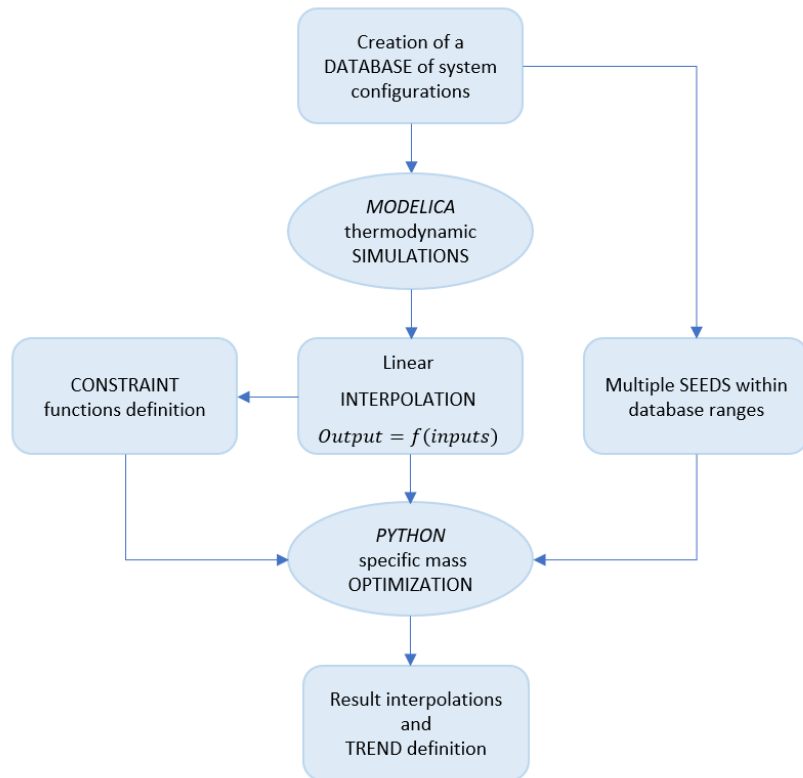


Figure 3.2: Diagram of the metamodeling and optimization procedure.

ple dimensions, a function relating an objective feature of the model to other variables is obtained [32]. The interpolant is constructed by triangulating the input data coming from the database of input variables, and performing linear barycentric interpolation on each triangle. Thereby, this method is employed to define the function to be optimized as well as the constraint functions, which in turn are used as inputs for the optimization. This last step is done using the *Sequential Least Squares Programming Algorithm* (SLSQP), an optimization method implemented once again inside the *SciPy* framework: by assigning to it a function to minimize, one or more constraints, variable boundary values, a computation limit (set to 1,000 iterations) and a starting value also called *seed*, eventually the algorithm would yield an optimal combination of the input variables. However, it's important to underline that the provided minimum is not necessarily the global one but only the minimum closer to the assigned seed. For this reason, the same procedure is performed using several starting points, spread between the highest and lowest input variable values present in the database. Once identified, the best set of operative conditions undergoes a final simulation in Modelica to verify the absence of any errors. To summarize, a scheme of the main steps that shape this optimization procedure has been displayed in fig. 3.2.

Thermal power level	Variable	Range of values
All thermal powers	Potassium inlet temperature [K]	810 - 890
	Potassium pressure [bar]	1.0 - 1.6
	Molten salt inlet temperature [K]	1,090 - 1,100
60 kWth	Molten salt flow rate [kg/s]	1.00 - 1.60
	Potassium flow rate [kg/s]	0.02 - 0.03
	Heat transfer area [m <sup>2</sup> ]	0.2 - 0.48
125 kWth	Molten salt flow rate [kg/s]	1.80 - 3.80
	Potassium flow rate [kg/s]	0.05 - 0.06
	Heat transfer area [m <sup>2</sup> ]	0.40 - 0.54
250 kWth	Molten salt flow rate [kg/s]	4.80 - 7.80
	Potassium flow rate [kg/s]	0.10 - 0.14
	Heat transfer area [m <sup>2</sup> ]	0.54 - 0.82
1 MWth	Molten salt flow rate [kg/s]	20 - 28
	Potassium flow rate [kg/s]	0.44 - 0.48
	Heat transfer area [m <sup>2</sup> ]	1.56 - 1.97

Table 3.3: Input variable ranges for the 1100 K molten salt inlet temperature database creation.

In principle, the procedure just described can be followed to optimize any system property. As long as the numerical tool is capable of finding a sufficiently robust function relating the target output with an array of variables, a similar method can be used for other parameters such as the total volume occupied by the system, the efficiency of the cycle, etc. This study only focuses on the power conversion system specific mass and to build the database, a first attempt was made by considering as inputs the following quantities: both sides mass flow rate and inlet temperature, secondary side pressure, boiler length, tubes number and internal diameter. Moreover, the inlet temperature on the potassium side is considered equal to the one at the turbine outlet, which at the same time sets the expansion ratio of the turbine itself. However, it was observed that the computational effort required by the linear interpolator algorithm increases almost exponentially with the number of variables to interpolate. A reasonable amount of time is needed for no more than six variables, therefore, the boiler and tube sizes were collapsed into a single quantity describing the heat transfer area.

Since various boiler geometries can correspond to a specific surface, a successive optimiza-



tion calculation is implemented in order to find the lighter heat exchanger configuration. Despite constituting a small percentage of the overall PCS weight, the mass of the latter is not included in the first optimization, which anyway ends up providing the heat transfer area yielding the minimum specific mass. That area is in turn used as the main constraint value for minimizing the boiler mass. Without any consideration of pressure load or turbulence instability, also a minimum cross section for the secondary side is put as a requirement and the same value of the ORNL boiler design is adopted [35]. Once the best size is found for the shell and tube, its contribute is added back to the overall specific mass.

In table 3.3, the variable ranges adopted to create the database for a molten salt inlet temperature of around 1,100 K are listed. It is important to underline that while increasing the power level, only the reported variables have been changed with respect to the ones related to the 60 MWth configuration. These intervals are also used to define the boundaries that the minimization algorithm receives as input. Even though the interpolated functions used either as optimization target and constraint are not defined outside of the convex hull of input points in the database, setting threshold values helps to speed up the numerical process.

### 3.1.4. Results

Once all the simulations have been run and the optimization process has terminated, the outcome configurations are analyzed in order to understand if some relations could be established.

Boiler mass scales quite linearly with the power produced, as presented in fig. 3.3a and this is a reflection of the dependence on the heat transfer area, which in turn is almost proportional to the thermal power exchanged along the boiler. It's noteworthy that for all the cases, the optimizer indicates the less-massive configuration as the one with tubes whose internal diameter and length are closer in values to the assigned lower bounds, whatever these can be. Through a subsequent analysis, it is demonstrated that, after imposing a minimum primary side cross section and fixing the tube and shell thickness, the quantity that less affects the boiler mass with the same heat transfer area is the number of tubes (fig. 3.3). Therefore, in this work, the length and internal diameter of the tubes are set to 2.50 m and 1 cm, respectively, in accordance with the ORNL design [35]. Future developments should include in the optimization also the effects of mechanical stress, thermal expansion and pressure loss, which are relevant to this component more than any other.

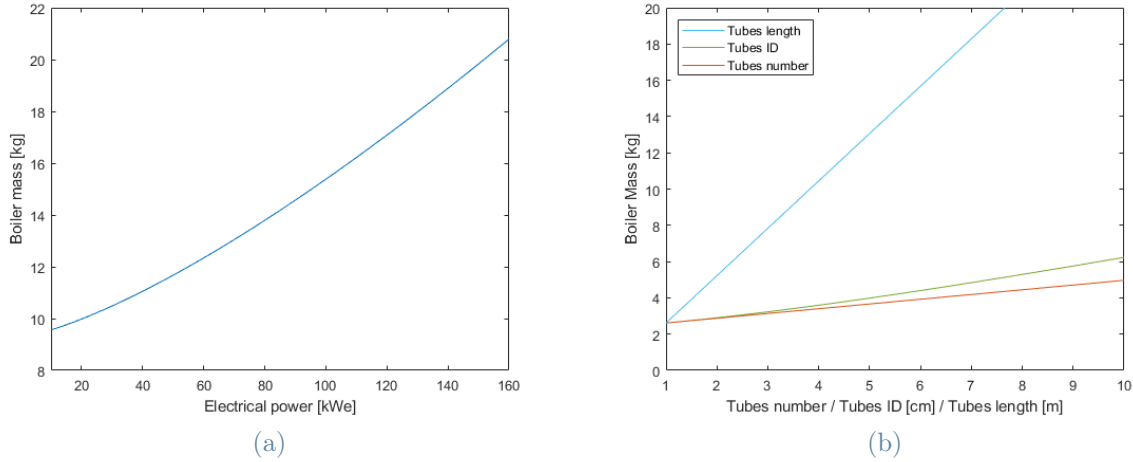


Figure 3.3: Boiler mass as function of electric power in fig. 3.3a. Boiler mass dependence on tubes number, internal diameter and length for same values of heat transfer area in fig. 3.3b.

By examining the outcomes of the heat rejection system in fig. 3.4a, it is evident that the specific mass trend follows the predictions. In the considered interval of values, for every power level an increase of temperature in the primary side of 100 K allows a savings of about half the unit mass thanks to a higher temperature of condensation.

Although a slightly decreasing behavior in the specific mass is also visible among different power levels having the same hot temperature, this benefit comes with a worsening of the overall cycle efficiency. As can be seen from the functions obtained through results interpolation in fig. 3.4b, despite the molten salt inlet temperature, high thermal power configurations are able to reach low specific mass values only at the expense of reducing the efficiencies down to 15%. In fact, when the mass flow rates are increased to assure a higher thermal power exchanged in the boiler, also the amount of heat the condenser must reject increases more or less proportionally (depending on the turbine exit quality). However, it is important to remind that these efficiency values are calculated considering an ideal power conversion between the turbine and alternator.

Since the HRS is the most massive component in the system and no efficiency requirement is posed, the optimization algorithm prefers to increase the cycle cold temperature, reducing the HRS mass, rather than find a more efficient configuration, increasing the electric power. Even if, in principle, a lower specific mass value is obtained by proceeding in this way, this might be an arguable decision when it comes to scaling the system to higher powers. These results might suggest that to enhance the power level without having to diminish the turbine exit temperature, strategies that increase efficiency are inevitable,

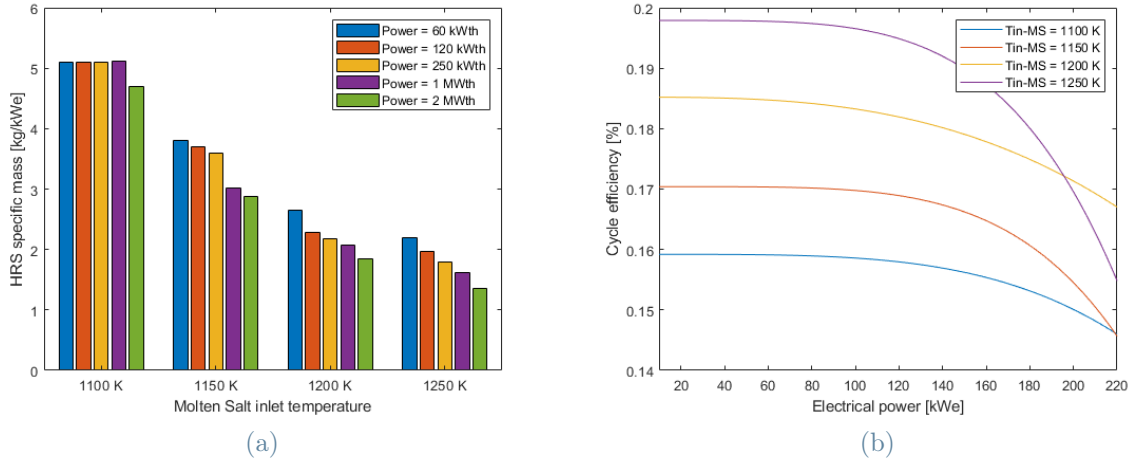


Figure 3.4: Heat rejection system specific mass (fig. 3.4a). Cycle efficiencies of the specific-mass-optimized configurations for different electric power levels (fig. 3.4b).

with both feed heating and reheating representing viable solutions. The former requires the adoption of a high-pressure turbine from which the potassium vapor is extracted and heated again before being returned to a low-pressure turbine. The second option implies exploiting the exhaust heat of the turbopump to preheat the primary fluid before it enters the boiler. However, the applicability of both techniques with a space Rankine cycle has yet to be verified.

Even if a way to extract more electricity from the same amount of thermal power was found, from the system mass point of view the heat rejection system would remain the determining factor for any conversion unit operating at more than 50 kWe. In fact, the comparison carried out in fig. 3.5 shows the different contributions to the specific mass of each component when the inlet temperature of the primary fluid is set to 1,200 K. As expected, the relative importance of every sub-system progressively reduces, except for the condenser and radiator. This demonstrates the existence of a limit to any space Rankine cycle mass optimization, which is established by the adopted heat rejection system. By relying on radiative heat transfer, the only way to improve the HRS capability seems to be to increase the primary side working temperature as much as possible.

This limit clearly reflects also on the system specific mass behaviour. Through interpolation of the optimal configuration specific masses, four distinct curves are obtained and reported in fig. 3.6. Once again the beneficial impact of a higher hot temperature is highlighted, however the steep decrease in specific mass that interests the relatively low power systems becomes more flat when the 100 kWe power threshold is overcome.

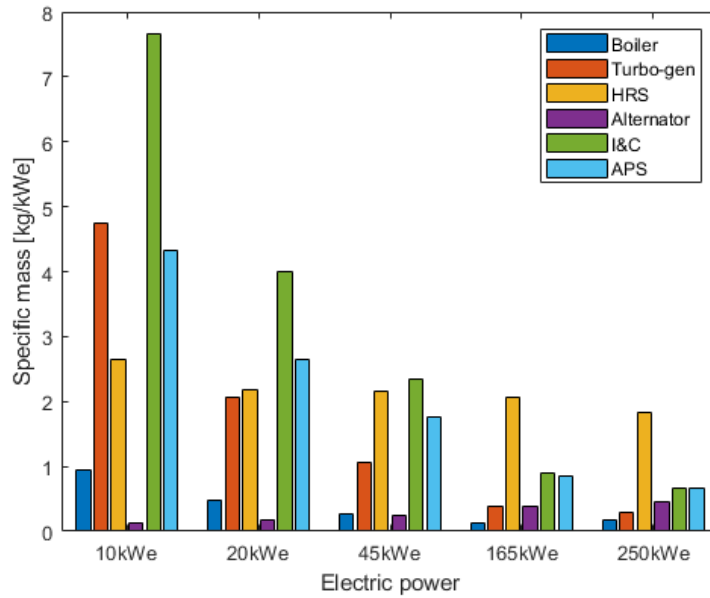


Figure 3.5: Contribution to the PCS specific mass by each component for different power levels with an inlet temperature of the primary side of 1,200 K.

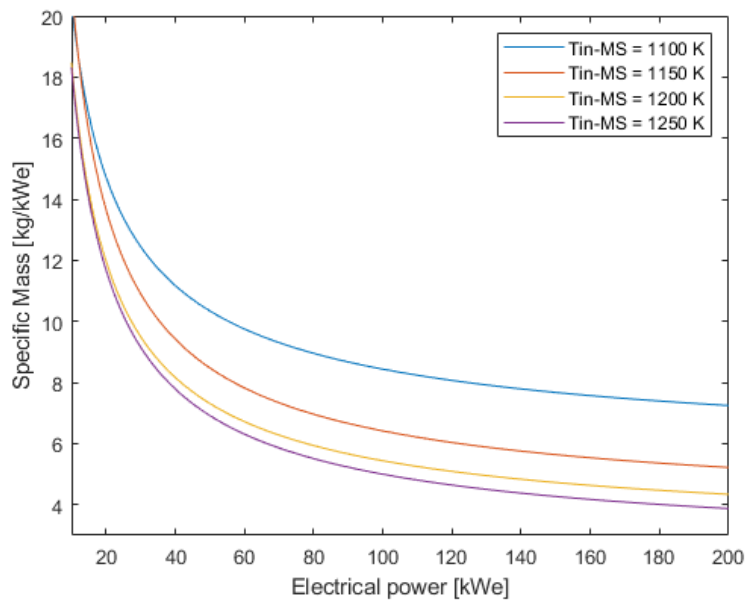


Figure 3.6: System overall specific mass as function of different power level and primary fluid inlet temperature.

Variable	Value
Thermal power	1 MW
Electric output	110 KWe
Primary side flow rate	24.02 kg/s
Secondary side flow rate	0.48 kg/s
Secondary side inlet temperature	948 K
Secondary side inlet pressure	2.86 bar

Table 3.4: 110 kWe potassium Rankine cycle system specifics obtained through an optimization procedure.

After having pointed out the trends resulting from the optimization of the different configurations, a conclusive study is done by applying the optimization procedure to some example power conversion systems. To do that, the molten salt reactor is supposed to be operated at its nominal power level of 1 MWth which ensures a core outlet fuel temperature of about 1,200 K. Moreover, an electric output within the applicability range of the power management and distribution system (100 KWe - 300 KWe) is required for the optimizer. In this way, the PMAD mass which has been so far neglected, can also be estimated. To give a more comprehensive evaluation of the whole propulsion unit, also the masses of molten fuel, reactor core cladding and reflector reported in table 1.1 are taken into account. To allow a more realistic analysis, the efficiency values suggested by ORNL for either the turbine and alternator, respectively of 74% and 0.88%, are adopted [35]. This implies a conversion efficiency of around 65%, here defined as the ratio between the electric output to the thruster and the mechanical power produced by the turbine.

The optimized configuration specifics are listed in table 3.4 whereas a summary of the estimated masses is presented in fig. 3.7a. An overall system mass of 3,862 kg is predicted for a 110 kWe system which corresponds to a PCS specific mass of 8.06 kg/kWe and an system one of 35.1 kg/kWe. The same procedure is then followed with equal considerations but requiring a minimum cycle efficiency. Starting from high values, the optimization process always failed, meaning that none of the configurations present within the interpolated ranges was able to reach such a high efficiency. By easing the demand from time to time, the algorithm is eventually able to find an optimized solution. In fact, a 150 kWe system of 4,657 kg with an efficiency of 15% and a PCS specific mass of 8.58 kg/Kwe and a system one of 31.0 kg/KWe is provided. This result allows for an important comment that remarks the importance of a coupled analysis. In fact, it is not granted that the power conversion system with the lowest specific mass, once combined with the nuclear reactor having the lowest specific mass, could represent the optimal

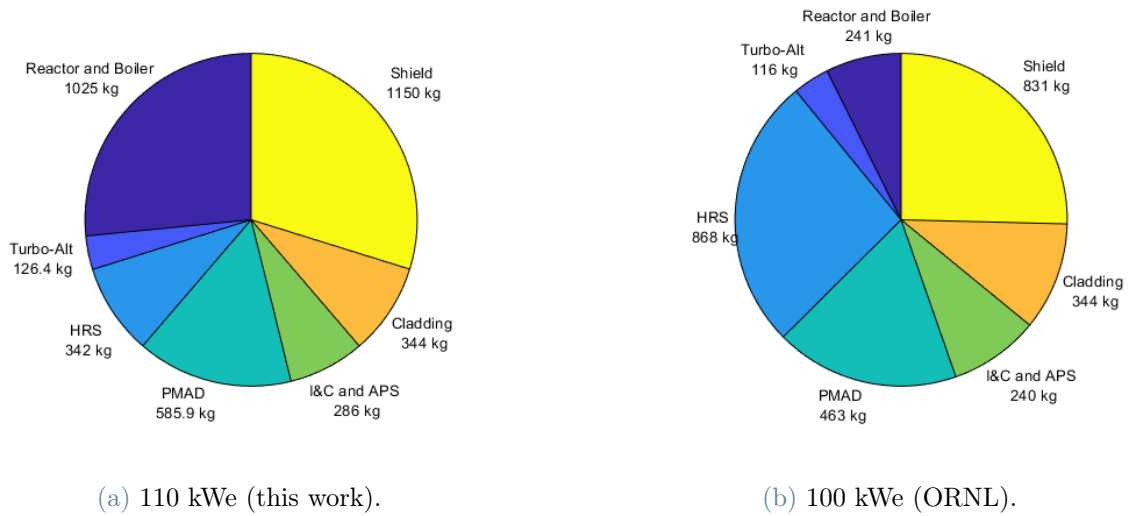


Figure 3.7: Major components estimated masses for potassium Rankine nuclear reactor power system.

solution. These two components are strictly related, and once again, a trade-off between mass and efficiency is crucial to design the best system.

In conclusion, the 110 kWe unit is compared to the one obtained at Oak Ridge, where a fast reactor fueled with highly enriched uranium in the form of solid uranium nitride was investigated. That design incorporates a power conversion system based on a 100 kWe potassium Rankine cycle in which lithium is the primary fluid. A hot temperature of 1350 K at the reactor outlet and a radiator one of 887 K, allow for 23.6% of cycle efficiency, without reheating solution at the expense of a 868 kg heavy heat rejection system (fig. 3.7b). A specific mass value of 30.7 kg/KWe is achieved with this configuration, which nevertheless relies on highly enriched fuel. This choice helps in considerably reducing the reactor mass but it is nowadays deemed an impracticable option due to non-proliferation reasons.

## 4 | Conclusions and future developments

The main objective of this thesis was to advance the development of a code that could outline the steps for the design of any nuclear electric propulsion system. This kind of complex problem prevents treating each branch as a separate entity. Interconnections must be identified and managed properly. One of these several connections, especially the one that links the nuclear power source and the power conversion system, was the goal of this investigation. A molten salt reactor was chosen as the best candidate among the several reactor concepts because of its many inherent qualities. On the other hand, the Rankine cycle is a strong option because of the ability of a liquid metal like potassium to work at extremely high temperatures combined with the necessity to reject heat as efficiently as possible. Therefore, determining how modifications to the former could affect the latter was the first accomplishment.

To do that, a metamodel that was able to establish functional relations between them was developed. This required creating a large database of system configurations, each characterized by a different set of operating states. The choice of five thermal power levels and four primary side inlet temperature conditions allowed for the inclusion and analysis of a wide range of design possibilities. All thermodynamic calculations were performed by means of a Modelica Rankine cycle model that was appropriately implemented and refined in order to be used with a potassium medium as well. A consistent part of the work was in fact devoted to finding appropriate state equations and heat transfer correlations for this working fluid, which in most cases was accomplished by recurring to experimental data interpolation. A comparative study with the results of either predictive numerical tools or experiments was conducted to validate it, and the results showed a strong agreement.

The primary importance of mass as a design factor for every component inside a spacecraft directs efforts toward estimating it. Volume evaluation or the adoption of reference unit designs were used to develop equations that assess the mass of every system component. The latter were added to the Modelica code so that multiple cycle simulations could be

run and give the overall weight of the conversion system and eventually its specific mass (kg/kWe). Through an analysis of the output results, it was shown that the specific mass trend of almost all the components tends to decrease linearly when the electric output is increased. A quite flat behavior was instead visible for the heat rejection system, which comprises heat pipes condenser and radiators. The way in which this component sets a limit to any possible mass reduction and the increasing of the hot cycle temperature as the only option to reject heat more efficiently were discussed. However, the relevance of trade-off considerations between system mass and cycle efficiency was highlighted after a successive optimization study.

As a result, this work went on to define how the functional relations established through the metamodeling process could be employed to assess an optimal Rankine configuration from the point of view of a specific mass. By striking a balance between accuracy and processing time, the use of numerical algorithms in the Python framework has thus proven to be successful for this work goal. Six input variables were recommended as the maximum for the multi-variable linear interpolator used to determine relationships between design configurations and output values, such as power, mass, etc. Whereas, regarding the minimize algorithm, the importance of boundary and constraint definition was emphasized. By reviewing the outcomes, the way in which the pursuit of the lowest possible specific mass Rankine configuration leads to a cycle efficiency worsening down to 12% for power levels above 50 KWe was observed. This demonstrated how the specific mass cannot be the only parameter to look at when trying to optimize such a power conversion system, with efficiency being an equally relevant factor.

At last, given the reported remarks, the optimization procedure was employed to assess the best Rankine cycle design for the nominal operating conditions of the molten salt reactor. By requiring a minimum cycle efficiency of 20% and including the reactor mass, a 3862 kg heavy system providing 110 kWe is obtained, which corresponds to a specific mass of 35.1 kg/kWe.

Even though the outlined procedure could be extended to different reactor concepts, slight adjustments would be needed. Nevertheless, this work was very preliminary and several assumptions were made for lack of better knowledge. If a feasible system is to be designed, the boiler is the component to which future research should devote great attention. The almost complete absence of long-lasting boiling tests carried out in microgravity or no-gravity conditions significantly limits the reliability of these studies. Moreover, mechanical stresses, thermal expansion effects, corrosion and erosion issues must be well predicted and properly accounted for when boiler configuration and material selection will be done. From a corrosion standpoint, the turbine is another very delicate unit and the impact of



adding moisture separators should be foreseen if potassium quality can not be kept high enough. In addition, part of the mass estimation work was done by employing component specifics borrowed from other research group studies, while the adoption of specifically designed technologies could improve the accuracy of the optimization.

Another important aspect that should be strongly emphasized is that of pressure losses. When dealing with two-phase liquid metals, not only frictional but also momentum drops should be investigated, with the heat exchanger being the most concerned unit due also to the presence of swirl generators. The molten salt side too, is no stranger to pressure loads that, together with fission gas effects, could have a significant influence on the pump mass and required power.

In conclusion, the achievements of this thesis allow for bridging the gap between two of the several components of a propulsion unit, but much remains to get the job done. A molten salt reactor combined with a Rankine-based power conversion system remains one of the most promising options for nuclear electric propulsion units and future improvements could make deep space exploration closer and closer.



## Bibliography

- [1] Beyondnerva.com, snap-50: The last of the snap reactors, <https://beyondnerva.com/2019/02/18/snap-50-the-last-of-the-snap-reactors/>.
- [2] Snap-50/spur program annual technical report, 1964. Technical report, Pratt and Whitney Aircraft, Middletown, Conn.(USA), 1964.
- [3] Snap-50/spur program annual technical report, 1964. 3 1964. doi: 10.2172/4315637. URL <https://www.osti.gov/biblio/4315637>.
- [4] F. Casella and A. Leva. Object-oriented modelling & simulation of power plants with modelica. In *Proceedings of the 44th IEEE Conference on Decision and Control*, pages 7597–7602. IEEE, 2005.
- [5] H. H. Coe. *Summary of thermophysical properties of potassium*. National Aeronautics and Space Administration, 1965.
- [6] H. W. Davison. *Compilation of thermophysical properties of liquid lithium*, volume 4650. National Aeronautics and Space Administration, 1968.
- [7] M. DeCrescente, M. Freed, and S. Caplow. Uranium nitride fuel development, snap-50. Technical report, Pratt and Whitney Aircraft, Middletown, Conn.(USA). Connecticut Advanced . . . , 1965.
- [8] T. J. Dolan. *Molten salt reactors and thorium energy*. Woodhead Publishing, 2017.
- [9] M. Eades, J. Flanders, N. McMurray, R. Denning, X. Sun, W. Windl, and T. Blue. Space molten salt reactor concept for nuclear electric propulsion and surface power. *Journal of the British Interplanetary Society*, 64:186–193, 2011.
- [10] C. Ewing, J. Stone, J. Spann, and R. Miller. High temperature properties of potassium. *Journal of Chemical and Engineering Data*, 11(4):460–468, 1966.
- [11] M. Garcia. Nasa astronauts train deep undersea for deep space missions, <https://www.nasa.gov/feature/nasa-astronauts-train-deep-undersea-for-deep-space-missions>.

- [12] Gen-4.org. The generation iv international forum, <https://www.gen-4.org/gif/>.
- [13] M. Gutstein, J. Peterson, and R. Weltmann. Thermal design procedures for space rankine cycle system boilers. In *IEEE INTERSOC. ENERGY CONVERSION ENG. CONF.*, number GESP-67, 1968.
- [14] P. Haubenreich, J. Engel, B. Prince, and H. Claiborne. Msre design and operations report. part iii. nuclear analysis. Technical report, Oak Ridge National Lab., Tenn., 1964.
- [15] J. A. Heller, G. J. Barna, and T. A. Moss. *Study of a 300-kilowatt Rankine-cycle Advanced Nuclear-electric Space-power System*. National Aeronautic and Space Administration, 1969.
- [16] R. Holcomb. Potassium rankine cycle nuclear power systems for spacecraft and lunar-mass surface power. Technical report, Oak Ridge National Lab., TN (United States), 1992.
- [17] A. Kuchibhotla, D. Banerjee, and V. Dhir. Forced convection heat transfer of molten salts: A review. *Nuclear Engineering and Design*, 362:110591, 2020.
- [18] R. N. Lyon. *Forced convection heat transfer theory and experiments with liquid metals*, volume 419. United States Atomic Energy Commission, Technical Information Service, 1949.
- [19] R. N. Lyon and H. Poppendiek. Liquid-metal heat transfer. *Liquid-metals Handbook*, page 184, 1951.
- [20] T. Masuda, H. Imai, and S. Korenaga. Thermodynamic properties of potassium. *The transactions of the Institute of Electrical Engineers of Japan. A*, 105(4):220–227, 1985.
- [21] X. Miao, H. Zhang, Q. Wang, Y. Xia, and W. Sun. Optimum design of nuclear electric propulsion spacecraft for deep space exploration. *Energy Reports*, 8:9629–9641, 2022.
- [22] I. Novikov, A. Solovyev, E. Khabakhpasheva, V. Gruzdev, A. Pridantsev, and M. Y. Vasenina. Heat transfer and thermophysical properties of molten alkali metals. *The Soviet Journal of Atomic Energy*, 1(4):545–560, 1956.
- [23] S. R. Oleson, L. M. Burke, L. S. Mason, E. R. Turnbull, S. Mccarty, A. J. Colozza, J. E. Fittje, J. T. Yim, M. Smith, T. W. Packard, et al. Compass final report: Nuclear electric propulsion (nep)-chemical vehicle 1.2. Technical report, 2021.
- [24] J. Pacio, L. Marocco, and T. Wetzel. Review of data and correlations for turbulent

- forced convective heat transfer of liquid metals in pipes. *Heat and Mass Transfer*, 51:153–164, 2015.
- [25] D. Poston et al. Fission-based electric propulsion for interstellar precursor mission. In *proceedings of Space Technology and Applications International Forum*, pages 974–983.
- [26] F. Quinteros, P. Rubiolo, V. Ghetta, J. Giraud, and N. Capellan. Design of a fast molten salt reactor for space nuclear electric propulsion. *Nuclear Science and Engineering*, pages 1–16, 2023.
- [27] H. Rouch, O. Geoffroy, P. Rubiolo, A. Laureau, M. Brovchenko, D. Heuer, and E. Merle-Lucotte. Preliminary thermal-hydraulic core design of the molten salt fast reactor (msfr). *Annals of Nuclear Energy*, 64:449–456, 2014.
- [28] K. Sands. The propulsion we’re supplying, it’s electrifying, <https://www.nasa.gov/feature/glenn/2020/the-propulsion-we-re-supplying-it-s-electrifying>.
- [29] P. M. Sforza. *Theory of aerospace propulsion*. Butterworth-Heinemann, 2016.
- [30] J. R. Stone. Alkali metal rankine cycle boiler technology challenges and some potential solutions for space nuclear power and propulsion applications. Technical report, 1994.
- [31] K. R. Supak. *Reduced gravity Rankine cycle system design and optimization study with passive vortex phase separation*. PhD thesis, Texas A&M University, 2008.
- [32] P. Virtanen, R. Gommers, T. E. Oliphant, M. Haberland, T. Reddy, D. Cournapeau, E. Burovski, P. Peterson, W. Weckesser, J. Bright, et al. Scipy 1.0: fundamental algorithms for scientific computing in python. *Nature methods*, 17(3):261–272, 2020.
- [33] M. Wall. Nasa, doe fund three nuclear thermal space propulsion concepts. *Space.com*, 2021.
- [34] C. Wang, J. Chen, S. Qiu, W. Tian, D. Zhang, and G. Su. Performance analysis of heat pipe radiator unit for space nuclear power reactor. *Annals of Nuclear Energy*, 103:74–84, 2017.
- [35] G. Yoder, J. Carbajo, R. Murphy, A. Qualls, C. Sulfredge, M. Moriarty, F. Widman, K. Metcalf, and M. Nikitkin. *Technology Development Program for an Advanced Potassium Rankine Power Conversion System Compatible with Several Space Reactor Designs*. United States. Department of Energy, 2005.



# A | Appendix A

Few constant properties are listed in table A.1 while afterwards equations to compute potassium saturation temperature are reported. It is worth underlining that these equations are independent of the phase state and that they are usable no matter if entropy or enthalpy is the input variable since they only depend on pressure, which is always an input.

Parameter	Values
Molar Mass MM [g/mol]	0.0391
Critical temperature [K]	2,223
Critical pressure [bar]	15.79

Table A.1: Potassium constant properties.

## A.1. Saturation temperature

Potassium saturation temperature (K) as function of pressure (Pa) for pressures below  $4 \cdot 10^5$  Pa (4 bar):

$$T_{sat} = 293.12 \cdot p^{0.1094} \quad R^2 = 0.9985 \quad (\text{A.1})$$

Potassium saturation temperature (K) as function of pressure (Pa) for pressures above  $4 \cdot 10^5$  Pa (4 bar):

$$T_{sat} = 3.2926 \cdot 10^{-30} \cdot p^5 - 3.6580 \cdot 10^{-23} \cdot p^4 + 3.6580 \cdot 10^{-16} \cdot p^3 - 3.7306 \cdot 10^{-10} \cdot p^2 + 5.8152 \cdot 10^{-4} \cdot p + 1.0210 \cdot 10^3 \quad R^2 = 0.9998 \quad (\text{A.2})$$

## A.2. Model explicit in pressure and enthalpy

## Liquid region

Potassium density ( $\frac{kg}{m^3}$ ) as function of temperature (K):

$$\rho_l = 900.77 - 0.21195 \cdot T - 3.4736 \cdot 10^{-5} \cdot T^2 + 1.6952 \cdot 10^{-8} \cdot T^3 \quad (A.3)$$

Potassium dynamic viscosity ( $Pa \cdot s$ ) as function of temperature (K):

$$\eta_l = 4.28 \cdot 10^{-1} \cdot T^{-1.16} \quad (A.4)$$

Potassium thermal conductivity ( $\frac{W}{m \cdot K}$ ) as function of temperature (K):

$$\lambda_l = 58.6563 - 2.8310 \cdot 10^{-3} \cdot T + 1.4799 \cdot 10^{-6} \cdot T^2 \quad (A.5)$$

Potassium specific heat at constant pressure ( $\frac{J}{kg \cdot K}$ ) as function of temperature (K) for temperatures below 300 K:

$$cp_l = 0.6321 \cdot T + 565.86 \quad R^2 = 0.9996 \quad (A.6)$$

Potassium specific heat at constant pressure ( $\frac{J}{kg \cdot K}$ ) as function of temperature (K) for temperatures above 300 K:

$$cp_l = 3.143 \cdot 10^{-4} \cdot T^2 - 4.886 \cdot 10^{-1} \cdot T + 950.7 \quad (A.7)$$

Potassium specific heat at constant volume ( $\frac{J}{kg \cdot K}$ ):

$$cv_l = cp_l \quad (A.8)$$

Potassium specific Entropy ( $\frac{J}{kg \cdot K}$ ) at saturation conditions as function of temperature (K):

$$S_l = 384.98 \cdot T^{0.2859} \quad R^2 = 0.9950 \quad (A.9)$$

Potassium specific Entropy ( $\frac{J}{kg \cdot K}$ ) outside the saturation curve as function of temperature



(K):

$$S = -3474.3 + 2189.0 \cdot \log_{10}T - 4.8899 \cdot 10^{-1} \cdot T + 1.5754 \cdot 10^{-4} \cdot T^2 \quad (\text{A.10})$$

Potassium temperature (K) as function of pressure (Pa) and specific Enthalpy ( $\frac{J}{kg}$ ) outside the saturation curve approximated as:

$$T(H, p) = T_{sat}(p) - \frac{H_l(p) - H}{cp} \quad (\text{A.11})$$

## Vapor region

Potassium density ( $\frac{kg}{m^3}$ ) as function of temperature (K):

$$\rho_v = 3.609 \cdot 10^{-6} \cdot e^{1.143 \cdot 10^{-2} \cdot T} \quad R^2 = 0.9900 \quad (\text{A.12})$$

Potassium dynamic viscosity ( $Pa \cdot s$ ) as function of temperature (K) :

$$\eta_v = 1.058 \cdot 10^{-8} \cdot T + 8.289 \cdot 10^{-6} \quad R^2 = 0.9976 \quad (\text{A.13})$$

Potassium thermal conductivity ( $\frac{W}{m \cdot K}$ ) as function of temperature (K):

$$\lambda_v = 7.570 \cdot 10^{-6} \cdot T + 6.262 \cdot 10^{-3} \quad R^2 = 0.9993 \quad (\text{A.14})$$

Isentropic expansion index as function of temperature (K):

$$\gamma_{is} = 2.955 \cdot T^{-0.102} \quad R^2 = 0.8881 \quad (\text{A.15})$$

Potassium specific heat at constant pressure ( $\frac{J}{kg \cdot K}$ ) calculated at 1150 K:

$$cp_v = 1149.8 \quad (\text{A.16})$$

Potassium specific heat at constant volume ( $\frac{J}{kg \cdot K}$ ) calculated as  $\frac{cp_v}{\gamma_{is}}$  :

$$cv_v = \frac{cp_v}{\gamma_{is}} \quad (A.17)$$

Potassium specific Entropy ( $\frac{J}{kg \cdot K}$ ) at saturated conditions as function of temperature (K):

$$S_v = 0.0011 \cdot T^2 - 3.7298 \cdot T + 7391.8 \quad R^2 = 0.9991 \quad (A.18)$$

Potassium specific Entropy ( $\frac{J}{kg \cdot K}$ ) as function of pressure (Pa) and temperature (K) outside the saturation curve approximated as:

$$S(p, T) = S_v(p) + cp \cdot \ln\left(\frac{T}{T_{sat}(p)}\right) \quad (A.19)$$

Potassium temperature (K) as function of pressure (Pa) and of specific Enthalpy ( $\frac{J}{K}$ ) outside the saturation curve approximated as:

$$T(H, p) = \frac{H - H_v(p)}{cp} + T_{sat}(p) \quad (A.20)$$

## Two-phase region

Potassium quality as function of specific Enthalpy ( $\frac{J}{K}$ ) :

$$x(H) = \frac{H - H_l}{H_v - H_l} \quad (A.21)$$

Potassium specific Entropy ( $\frac{J}{kg \cdot K}$ ):

$$S = S_l + x \cdot (S_v - S_l) \quad (A.22)$$

Potassium specific heat at constant pressure ( $\frac{J}{kg \cdot K}$ ) :

$$cp = cp_l + x \cdot (cp_v - cp_l) \quad (A.23)$$

Potassium specific heat at constant volume ( $\frac{J}{kg \cdot K}$ ) calculated as  $\frac{cp_v}{\gamma_{is}}$  :

$$cv = \frac{cp}{\gamma_{is}} \quad (\text{A.24})$$

Potassium density ( $\frac{kg}{m^3}$ ):

$$\rho_{bi} = \rho_v + \rho_l \cdot (1 - x) \quad (\text{A.25})$$

### A.3. Model explicit in pressure and entropy

#### Liquid region

Potassium specific heat at constant pressure ( $\frac{J}{kg \cdot K}$ ) calculated at 950 K:

$$cp_l = 795 \quad (\text{A.26})$$

Potassium specific Entropy ( $\frac{J}{kg \cdot K}$ ) at saturation conditions as function of pressure (Pa):

$$S_l = 1936.7 \cdot p^{0.0323} \quad R^2 = 0.9887 \quad (\text{A.27})$$

Potassium temperature (K) as function of pressure (Pa) and specific Entropy ( $\frac{J}{kg \cdot K}$ ) approximated as:

$$T = T_{sat}(p) \cdot e^{\frac{S - S_l}{cp_l}} \quad (\text{A.28})$$

Potassium specific Enthalpy ( $\frac{J}{kg}$ ) as function of pressure (Pa) and specific Entropy ( $\frac{J}{kg \cdot K}$ ) approximated as:

$$H = H_l(p) + cp_l \cdot (T(p, S) - T_{sat}) \quad (\text{A.29})$$

Potassium specific Enthalpy ( $\frac{J}{kg}$ ) for saturated liquid as function of pressure (Pa) for pressures below  $4 \cdot 10^5$  Pa ( 4 bar ):

$$H_l = 224575 \cdot p^{0.114} \quad R^2 = 0.9981 \quad (\text{A.30})$$

Potassium specific Enthalpy ( $\frac{J}{kg}$ ) for saturated liquid as function of pressure (Pa) for pressures above  $4 \cdot 10^5$  Pa ( 4 bar ):

$$H_l = -2.010 \cdot 10^{-8} \cdot p^2 + 2.041 \cdot 10^{-1} \cdot p + 9.127 \cdot 10^5 \quad R^2 = 0.9965 \quad (\text{A.31})$$

## Vapor region

Potassium specific Entropy ( $\frac{J}{kg \cdot K}$ ) at saturation conditions as function of pressure (Pa):

$$S_v = 7121.8 \cdot p^{-0.037} \quad R^2 = 0.9996 \quad (\text{A.32})$$

Potassium temperature (K) as function of pressure (Pa) and specific Entropy ( $\frac{J}{kg \cdot K}$ ) approximated as:

$$T = T_{sat}(p) \cdot e^{\frac{S-S_v}{cp_v}} \quad (\text{A.33})$$

Potassium specific Enthalpy ( $\frac{J}{kg}$ ) as function of pressure (Pa) and specific Entropy ( $\frac{J}{kg \cdot K}$ ) approximated as:

$$H = H_v(p) + cp_v \cdot (T(p, S) - T_{sat}) \quad (\text{A.34})$$

Potassium specific Enthalpy ( $\frac{J}{kg}$ ) at saturation conditions as function of pressure (Pa) for pressures below  $4 \cdot 10^5$  Pa ( 4 bar ):

$$H_v = 2535011 \cdot p^{0.01} \quad R^2 = 0.9949 \quad (\text{A.35})$$

Potassium specific Enthalpy ( $\frac{J}{kg}$ ) at saturation conditions as function of pressure (Pa) for pressures above  $4 \cdot 10^5$  Pa ( 4 bar ):

$$H_v = -9.359 \cdot 10^{-9} \cdot p^2 + 6.332 \cdot 10^{-2} \cdot p + 2.773 \cdot 10^6 \quad R^2 = 0.9996 \quad (\text{A.36})$$

## Two-phase region

Potassium vapour quality as function of specific Entropy ( $\frac{J}{kg \cdot K}$ ):

$$x(S) = \frac{S - S_l}{S_v - S_l} \quad (\text{A.37})$$

Potassium specific Entropy ( $\frac{J}{kg \cdot K}$ ):

$$H = H_l + x \cdot (H_v - H_l) \quad (\text{A.38})$$



# B | Appendix B

Most of the Lithium properties have been treated as constant values except for dynamic viscosity and thermal conductivity whose describing equations were recovered by the following report:

- Harry W. Davison, "Compilation of thermophysical properties of liquid Lithium", NASA, Lewis Research Center, Cleveland, Ohio (July 1968) [6]

For both the correlations a dependence on Lithium temperature has been adopted.

Variables	Values
Molar Mass MM [g/mol]	0.00694
Specific heat capacity $C_p$ [J/kg·K]	4,169
Density [kg/m <sup>3</sup> ]	512
Isobaric Expansion Coefficient $\beta$ [K <sup>-1</sup> ]	$0.46 \cdot 10^{-4}$

Table B.1: Lithium constant properties.

Lithium dynamic viscosity ( $Pa \cdot s$ ) as function of temperature (K):

$$\eta = e^{-3.08 + \frac{57.63}{T} - 5.172 \cdot 10^{-4} \cdot T} \quad (\text{B.1})$$

Lithium thermal conductivity ( $\frac{W}{m \cdot K}$ ) as function of temperature (K):

$$\lambda = 21.874 + 0.056255T - 1.8325 \cdot 10^{-5}T^2 \quad (\text{B.2})$$



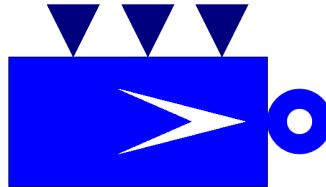


# C | Appendix C

## C.1. Modelica components

Here is a list of the components used for the Rankine Cycle model implemented inside the Modelica environment. Most of them have been taken by the ThermoPower library developed in 2003 by professor Francesco Casella at Politecnico of Milan [4]. The most important equations solved by each component are presented too.

### C.1.1. Source Mass Flow



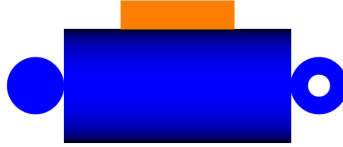
This component is used to set a flow rate source to the fluid.

INPUT:

- $w$  nominal mass fowrate [kg/s]
- $p$  nominal pressure [Pa]
- $G$  hydraulic conductance [(kg/s)/Pa]
- $T$  nominal temperature [K]
- $h$  nominal specific enthalpy [J/kg]

Nominal temperature and nominal specific enthalpy cannot be given both as input value. Once a value is set the other is calculated accordingly through the correlations.

### C.1.2. Flow-1DFV-2ph



This component is a one-dimensional fluid flow model for either one-phase or two-phase mixture. In case of two-phase flow, the same velocity is assumed for both phases (homogeneous model). Uniform velocity is assumed on the cross section, leading to a 1-D distributed parameter model. The fluid flow can exchange thermal power through the lateral surface, which is represented by the wall connector. The mass, momentum, and energy balance equation are discretized with the finite volume method. The state variables are one pressure, one flow rate (optional) and  $N-1$  specific enthalpies.

INPUT:

- $N$  number of nodes for thermal variables
- $N_w$  number of volumes on the wall interface
- $N_t$  number of tubes in parallel
- $l$  tube length [m]
- $H$  elevation of outlet over inlet [m]
- $A$  cross sectional area (single tube) [ $m^2$ ]
- $\omega$  perimeter of heat transfer surface (single tube) [m]
- $D_{hyd}$  hydraulic diameter (single tube) [m]
- $K f_{nom}$  nominal hydraulic resistance coefficient

INITIALISATION:

- fluid phase
- pressure start value [Pa]
- inlet enthalpy start value [J/kg]
- outlet enthalpy start value [J/kg]

## HEAT TRANSFER:

- $kc$  correction factor for heat transfer
- $\gamma_{liq}$  nominal heat transfer coefficient, liquid phase [W/(m<sup>2</sup>·K)]
- $\gamma_{2ph}$  nominal average heat transfer coefficient, two-phase [W/(m<sup>2</sup>·K)]
- $\gamma_{vap}$  nominal heat transfer coefficient, vapour phase [W/(m<sup>2</sup>·K)]

The heat transfer is by default implemented through the *FlowDependentHeatTransferCoefficient2ph* model which calculates the heat exchanged between the fluid and the wall for each finite volume after the equation:

$$Qw = (T_{wall} - T_{vol}) \cdot \omega \cdot l \cdot Nt \cdot \gamma \cdot kc \quad (C.1)$$

where  $T_{wall}$  and  $T_{vol}$  are the internal wall temperature (K) and the fluid temperature (K) respectively, while the correct  $\gamma$  value is selected after having identified the state of the fluid through an enthalpy evaluation. At this point mass, momentum and energy balance can be solved for each volume:

$$\frac{dM[j]}{dt} = A \cdot l \cdot \left( \frac{d\rho[j]}{dh_l} \cdot \frac{dh[j]}{dt} + \frac{d\rho[j]}{dh_r} \cdot \frac{dh[j+1]}{dt} + \frac{d\rho[j]}{dp} \cdot \frac{dp}{dt} \right) \quad (C.2)$$

$$\frac{l}{A} \cdot \frac{dw}{dt} + (p_{out} - p_{in}) + Dp_{stat} + Dp_{fric} = 0 \quad (C.3)$$

$$A \cdot l \cdot \rho[j] \cdot \frac{dh[j]}{dt} + w[j] \cdot (h[j+1] - h[j]) - A \cdot l \cdot \frac{dp}{dt} = \frac{Qw}{Nt}[j] \quad (C.4)$$

where  $j$  is the index of each finite volume,  $dh_l$  and  $dh_r$  the derivative with respect to the enthalpy of the left side volume and of the right side volume respectively. Even if they have been included in the momentum balance, pressure drop due to static head  $Dp_{stat}$  and to friction  $Dp_{fric}$  have been neglected in this model.

### C.1.3. Metal-Tube-FV



This component is the model of a cylindrical tube of solid material. The heat capacity (which is lumped at the center of the tube thickness) is accounted for, as well as the thermal resistance due to the finite heat conduction coefficient. Longitudinal heat conduction is neglected.

INPUT:

- $Nw$  number of volumes on the wall interface
- $Nt$  number of tubes in parallel
- $l$  tube length [m]
- $r_{int}$  internal radius (single tube) [m]
- $r_{ext}$  external radius (single tube) [m]
- $\rho_{mcm}$  metal heat capacity per unit volume [ $\text{J}/\text{m}^3 \cdot \text{K}$ ]
- $\lambda$  thermal conductivity [ $\text{W}/\text{m} \cdot \text{K}$ ]

INITIALISATION:

- $T_{start,ar}$  average temperature [K]
- $T_{start1}$  temperature start value - first volume [K]
- $T_{startN}$  temperature start value - last volume [K]

Thanks to the following equations heat conduction over the wall thickness is evaluated:

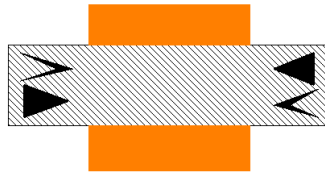
$$\frac{l}{Nw \cdot Nt} \cdot \rho_{mcm} \cdot Am \cdot \frac{dT}{dt} = Q_{int} + Q_{ext} \quad (\text{C.5})$$

$$Q_{int} = \lambda \cdot 2 \cdot \pi \cdot \frac{l}{Nw} \cdot \frac{Tw_{int} - T_{vol}}{\log\left(\frac{r_{int} + r_{ext}}{2 \cdot r_{int}}\right)} \cdot Nt \quad (C.6)$$

$$Q_{ext} = \lambda \cdot 2 \cdot \pi \cdot \frac{l}{Nw} \cdot \frac{Tw_{ext} - T_{vol}}{\log\left(\frac{2 \cdot r_{ext}}{r_{int} + r_{ext}}\right)} \cdot Nt \quad (C.7)$$

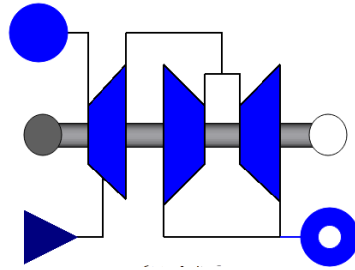
The first one is an energy balance equation in which  $Am = (r_{ext}^2 - r_{int}^2) \cdot \pi$ . The other equations describe heat conduction through the internal half-thickness and through the external half-thickness respectively.

#### C.1.4. Counter-Current-FV



This component is used to model counter-current heat transfer. The temperature and flux vectors on one side are swapped with respect to the other side. This means that the temperature of node  $j$  on side 1 is equal to the temperature of node  $N-j+1$  on side 2; heat fluxes behave correspondingly.

### C.1.5. Steam-Turbine-Unit



This model describes a simplified steam turbine unit, with a high pressure and a low pressure turbine. The inlet flow rate is proportional to the inlet pressure and to simulate throttling one could insert a valve before the turbine unit inlet. The model assumes that a fraction of the available hydraulic power is converted by the HP turbine while the remaining part is converted by the LP turbine, however in our simplified case the HP fraction is set to unit. This model does not include any shaft inertia by itself but if needed it's possible to add a *Modelica.Mechanics.Rotational.Inertia* model to one of the shaft connectors.

INPUT:

- $p$  inlet nominal pressure [Pa]
- $w$  inlet nominal flow rate [kg/s]
- $\eta_{iso}$  isentropic efficiency (per unit)
- $HP - fraction$  fraction of power provided by the HP turbine (per unit)
- $T_{HP}$  time constant of HP mechanical power response [s]
- $T_{LP}$  time constant of LP mechanical power response [s]

INIZIALISATION:

- $p_{startin}$  inlet start pressure [Pa]
- $w_{start}$  flow rate start value [kg/s]
- $h_{startin}$  inlet enthalpy start value [J/kg]
- $h_{startout}$  outlet enthalpy start value [J/kg]

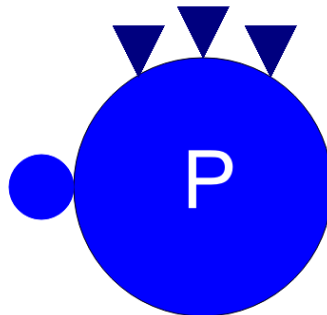
The turbine model is used to obtain an estimation of the mechanical power  $P_m$  that is possible to extract from the fluid, solving the following equations:

$$h_{in} - h_{out} = \eta_{iso} \cdot (h_{in} - h_{iso}) \quad (C.8)$$

$$P_m = \eta_{mech} \cdot w \cdot (h_{in} - h_{out}) \quad (C.9)$$

where  $h_{iso}$  is the fluid isentropic enthalpy calculated (through the correlations) as function of inlet entropy and outlet pressure.

### C.1.6. Sink-Pressure



This component is a pressure sink for fluid flow. When the *hydraulic resistance*  $R$  is set to zero, it behaves as an ideal sink, otherwise the inlet pressure increases proportionally to the incoming flow rate.

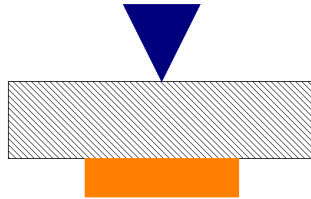
INPUT:

- $p$  nominal pressure [Pa]
- $R$  hydraulic resistance [Pa/(kg/s)]
- $T$  nominal temperature [K]
- $h$  nominal specific enthalpy [J/kg]

As for the mass flow rate source, nominal temperature and nominal specific enthalpy

cannot be given both as input value. Once a value is set the other is calculated accordingly through the correlations.

### C.1.7. Heat-Source-1DFV



This is the model of an ideal tubular heat flow source, with uniform heat flux. A power signal connector is used to provide it the actual heating power. In our model a negative power value is used in order to simulate an heat sink.

INPUT:

- $N_w$  number of volumes on the wall interface



## List of Figures

1.1	Layout rendering of the space MSR core with a fast spectrum [26]. . . . .	15
1.2	Reactivity swing of the LEU fast MSR due to the fuel burnup. Reactor thermal power set to 1 MW over the 10 years of operating time [26]. . . . .	17
1.3	Reactivity swing over time with different boron concentrations [26]. . . . .	18
1.4	Maximum and minimum reactivity swing as function of boron concentration [26]. . . . .	18
2.1	System specific mass as function of electric power produced [31]. . . . .	24
2.2	Rankine cycle schematic. . . . .	25
2.3	Circular-arc shaped once-through boiler with swirl generators. . . . .	26
2.4	Cyclone boiler design. . . . .	27
2.5	Heat pipe longitudinal section. . . . .	28
2.6	Schematic of a heat rejection system portion. . . . .	29
2.7	Typical distribution of heat transfer coefficient in a Potassium heated counterflow boiler tube [13]. . . . .	32
2.8	Two phase local heat transfer coefficient of Potassium obtained through a serpentine-boiler experiment carried out by Pratt & Whitney Aircraft in 1964 [3]. . . . .	33
2.9	Heat transfer coefficient distribution of a 3.3 MW boiler design implemented in Modelica. . . . .	34
2.10	Overall heat transfer coefficient distribution for a 3.3 MW Nb-1%Zr boiler design with lithium at the shell side and potassium at the tube side [13]. . . . .	37
2.11	Comparison of temperature distribution in a 2 MWth once-through potassium boiler design for advance Rankine space-power system [15]. . . . .	39
2.12	Comparison of temperature distribution in a 3 MWth once-through example boiler design [13]. . . . .	40
2.13	Heat rejection system mass scaling as function of turbine exit temperature with different heat loads to be rejected. . . . .	43
2.14	Mass scaling of feed pump (a), turbo-generator and alternator (b). . . . .	45

3.1	Rankine cycle layout in the Modelica environment. . . . .	48
3.2	Diagram of the metamodeling and optimization procedure. . . . .	55
3.3	Boiler mass as function of electric power in fig. 3.3a. Boiler mass dependence on tubes number, internal diameter and length for same values of heat transfer area in fig. 3.3b. . . . .	58
3.4	Heat rejection system specific mass (fig. 3.4a). Cycle efficiencies of the specific-mass-optimized configurations for different electric power levels (fig. 3.4b). . . . .	59
3.5	Contribution to the PCS specific mass by each component for different power levels with an inlet temperature of the primary side of 1,200 K. . . .	60
3.6	System overall specific mass as function of different power level and primary fluid inlet temperature. . . . .	60
3.7	Major components estimated masses for potassium Rankine nuclear reactor power system. . . . .	62

## List of Tables

1.1	Main MSR parameters [26]. . . . .	16
2.1	Verified ranges of applicability of the reported equations. . . . .	24
2.2	Applicability ranges of the correlations implemented in the computer program used to obtain the heat transfer coefficient distribution of fig. 2.7. . . . .	33
2.3	Range of experimental test conditions of fig. 2.8. . . . .	33
2.4	LiF-UF <sub>4</sub> properties kept constant in the model. . . . .	36
2.5	Forced convection correlations for flow in circular pipes. . . . .	36
2.6	Design specifics for a 2 MWth once-through potassium boiler developed by NASA in 1969 [15]. . . . .	39
2.7	Design specifics for a 3 MWth once-through boiler developed by J.R Peterson in 1968 [13]. . . . .	41
3.1	Rankine cycle component models in Modelica . . . . .	50
3.2	List of the Rankine cycle model parameters kept fixed for all the simulations. . . . .	52
3.3	Input variable ranges for the 1100 K molten salt inlet temperature database creation. . . . .	56
3.4	110 kWe potassium Rankine cycle system specifics obtained through an optimization procedure. . . . .	61
A.1	Potassium constant properties. . . . .	71
B.1	Lithium constant properties. . . . .	79



## List of Symbols

Variable	Description	SI unit
$C_p$	specific heat capacity	$\text{m}^2/\text{s}^2\text{K}$
$cp_l$	liquid specific heat	$\text{J}/\text{kg}\cdot\text{K}$
$cp_v$	vapor specific heat	$\text{J}/\text{kg}\cdot\text{K}$
$cv_l$	liquid specific heat at constant volume	$\text{J}/\text{kg}\cdot\text{K}$
$d$	pipe internal diameter	m
$D_e$	external diameter	m
$D_{eq}$	equivalent diameter	m
$D_i$	internal diameter	m
$D_o$	pipe outer diameter	m
$\Delta P$	pump pressure rise	Pa
$E$	eddy diffusivity of heat to eddy diffusivity of momentum ratio	m
$\eta$	thrust efficiency	%
$\eta_l$	liquid dynamic viscosity	$\text{Pa}\cdot\text{s}$
$\eta_v$	vapor dynamic viscosity	$\text{Pa}\cdot\text{s}$
$G$	pump drive flow rate	$\text{kg}/\text{s}$
$g_o$	gravitational acceleration at sea level	$\text{m}/\text{s}^2$
$\gamma_{insert}$	insert heat transfer enhancing multiplier	
$\gamma_{HRS}$	heat rejection system mass to heat-to-reject ratio	$\text{kg}/\text{W}$
$\gamma_{is}$	isentropic expansion index	
$h_{SV}$	superheated vapor heat transfer coefficient	$\text{W}/\text{m}^2\cdot\text{K}$
$h_{SL}$	subcooled liquid heat transfer coefficient	$\text{W}/\text{m}^2\cdot\text{K}$
$h_{NB}$	nucleate boiling heat transfer coefficient	$\text{W}/\text{m}^2\cdot\text{K}$
$h_{max}$	potassium heat transfer coefficient at CHF	$\text{W}/\text{m}^2\cdot\text{K}$

Variable	Description	SI unit
$h_{dew}$	subcooled liquid heat transfer coefficient at dew point	W/m <sup>2</sup> ·K
$h_{Li}$	lithium heat transfer coefficient	W/m <sup>2</sup> ·K
$h_{insert}$	superheated vapor heat transfer coefficient in pipe with inserts	W/m <sup>2</sup> ·K
$H_l$	liquid specific enthalpy	J/kg
$H_v$	vapor specific enthalpy	J/kg
$I_{sp}$	specific impulse	kg/N·s
$J$	total current	Ampere
$K$	thermal conductivity	W/m·K
$K_{SL}$	subcooled liquid thermal conductivity	W/m·K
$L$	axial length	m
$L_H$	helical length	m
$\lambda$	lithium thermal conductivity	W/m·K
$M_{HRS}$	heat rejection system mass	kg
$M_{pump}$	feed pump mass	kg
$M_{turb}$	turbine mass	kg
$M_{alternator}$	alternator mass	kg
$M_{PMAD}$	power management and distribution mass	kg
$M_{I\&C}$	instrumentation and control mass	kg
$M_{APS}$	auxiliary power system mass	kg
$m$	propellant mass flow rate	kg/s
$N$	alternator operating speed	rpm
$N_{pump}$	turbo-pump speed	rpm
$N_{turb}$	turbine speed	rpm
$Nu$	Nusselt number	
$Q'''$	core average power density	kW/m <sup>3</sup>
$p$	pipe internal pressure	Pa
$P$	total thruster power	kW
$P_{hyd}$	pump hydraulic power	
$Pe$	Péclet number	
$P_e$	electric power	kWe

Variable	Description	SI unit
$P_m$	turbine shaft power	kW
$Pr$	Prandtl number	
$Pr_l$	mean turbulent Prandtl number	
$pf$	alternator power factor	
$Q_R$	core power	kW
$Q_{Rej}$	condenser heat to reject	W
$R$	shell radius	m
$Re$	Reynolds number	
$\rho$	density	kg/m <sup>3</sup>
$\rho_l$	liquid density	kg/m <sup>3</sup>
$\rho_v$	vapor density	kg/m <sup>3</sup>
$S_l$	liquid specific entropy	J/kg·K
$S_v$	vapor specific entropy	J/kg·K
$S_m$	allowable stress	MPa
$t_m$	minimum thickness	m
$T$	engine thrust	N
$T_{out}$	turbine exit temperature	K
$T_{sat}$	saturation temperature	K
$t$	pipe thickness	m
$u_e$	exhaust velocity	m/s
$\mu_b$	bulk fluid dynamic viscosity	Pa·s
$\mu_w$	fluid dynamic viscosity at the wall	Pa·s
$V$	voltage	V
$V_{core}$	reactor core volume	m <sup>3</sup>
$x$	pitch to diameter ratio	
$x$	vapor quality	%





## Acknowledgements

Mi piacerebbe concludere questo lavoro ringraziando tutte le persone che hanno contribuito a portarlo a termine. Innanzitutto il Professor Lorenzi per essere stato il mio punto di riferimento, per essersi speso nel rendere possibile questa esperienza e non avermi mai fatto mancare la sua disponibilità e il suo supporto. My special thanks to Professor Rubiolo and all his colleagues at LPSC for welcoming me, giving me a taste of France and Argentina and helping shape my future. Un grazie immenso ai miei genitori senza i quali nulla di questo sarebbe esistito. Vi sono grato per aver creduto in me incondizionatamente e spero di avervi resi felici e orgogliosi tanto quanto voi avete reso con me. Ringrazio di cuore Maria per essere stata sempre al mio fianco, per avermi ispirato con la sua audacia, il suo coraggio e il suo affetto e per avermi insegnato che nella vita non conta ciò che accade ma come si reagisce. Un ringraziamento sentito a tutti i miei amici di paese perchè con i loro consigli hanno segnato la mia strada e con il loro calore mi hanno permesso di seguirla. Ringrazio i miei compagni Giacomo, Francesco e Valerio per aver condiviso con me i primi tre anni di corsi, di pranzi e di risate al Politecnico. Un grazie anche a Guido, Sophie, Alessandro, Michele e agli altri ragazzi del dipartimento di nucleare per avermi regalato i loro consigli e il loro entusiasmo che hanno reso unica ogni giornata trascorsa insieme. Una dedica speciale a Matteo, il mio compagno di viaggio, la *chat* più spassosa del mio cellulare e il miglior amico con cui potessi trascorrere questi cinque anni. Infine un grazie doveroso a Beppe per l'abilità con cui ha arricchito di disegni questa tesi.

